Naval Ocean Systems Center
San Diego, CA 92152-5000

AD-A214 765

Technical Document 1658
September 1989

Optical Transmission Through Clouds

Cubic Cloud Model and Simulation

Titan Systems, Inc.

The views and conclusions contained in this report are those of the contractors and should not be interpreted as representing the official policies, either expressed or implied, of the Naval Ocean Systems Center or the U.S. Government.

Approved for public release; distribution is unlimited.

NAVAL OCEAN SYSTEMS CENTER

San Diego, California 92152-5000

E. G. SCHWEIZER, CAPT, USN
Commander

R. M. HILLYER
Technical Director

ADMINISTRATIVE INFORMATION

This work was performed for Defense Advanced Research Projects Agency, 1400 Wilson Boulevard, Arlington, VA 22209 under program element 0603226E. Contract N66001-87-D-0133 was carried out by Titan Systems, Inc., 9191 Towne Centre Road, Suite 500, San Diego, CA 92122, under the technical coordination of L. C. Russel, Electro-Optic Systems Branch, Code 844, Naval Ocean Systems Center, San Diego, CA 92152-5000.

Released by
R. P. Schindler, Head
Electro-Optic Systems Branch

Under authority of
M. S. Kvigne, Head
Satellite Communications
Division

FS

UNCLASSIFIED

SECURITY CLASSIFICATION OF THIS PAGE

REPORT DOCUMENTATION PAGE

1a REPORT SECURITY CLASSIFICATION UNCLASSIFIED	1b RESTRICTIVE MARKINGS
2a. SECURITY CLASSIFICATION AUTHORITY	3 DISTRIBUTION/AVAILABILITY OF REPORT Approved for public release; distribution is unlimited
2b DECLASSIFICATION/DOWNGRADING SCHEDULE	
4 PERFORMING ORGANIZATION REPORT NUMBER(S)	5 MONITORING ORGANIZATION REPORT NUMBER(S) NOSC TD 1658
6a NAME OF PERFORMING ORGANIZATION Titan Systems, Inc.	6b OFFICE SYMBOL (if applicable)
7a NAME OF MONITORING ORGANIZATION Naval Ocean Systems Center	
6c ADDRESS (City, State and ZIP Code) 9191 Towne Centre Road, Suite 500 San Diego, CA 92122	7b ADDRESS (City, State and ZIP Code) San Diego, CA 92152-5000
8a NAME OF FUNDING/SPONSORING ORGANIZATION Defense Advanced Research Projects Agency	8b OFFICE SYMBOL (if applicable)
9 PROCUREMENT INSTRUMENT IDENTIFICATION NUMBER N66001-87-D-0133	
8c ADDRESS (City, State and ZIP Code) 1400 Wilson Boulevard Arlington, VA 22209	10. SOURCE OF FUNDING NUMBERS

PROGRAM ELEMENT NO	PROJECT NO	TASK NO	AGENCY ACCESSION NO
0603226E	CH40		DN307 441

11. TITLE (include Security Classification)

OPTICAL TRANSMISSION THROUGH CLOUDS
Cubic Cloud Model and Simulation

12. PERSONAL AUTHOR(S)

13a. TYPE OF REPORT	13b TIME COVERED	14 DATE OF REPORT (Year, Month, Day)	15 PAGE COUNT
Final	FROM TO	September 1989	93

16. SUPPLEMENTARY NOTATION

17 COSATI CODES			18 SUBJECT TERMS (Continue on reverse if necessary and identify by block number)
FIELD	GROUP	SUB-GROUP	optical communications radiative transfer

19 ABSTRACT (Continue on reverse if necessary and identify by block number)

This report is part of an ongoing effort to characterize clouds. Analytic models have been developed for cloud transmission and simulations have been carried out for spatial and temporal spreading. A simulation was developed for radiative transfer in finite clouds in order to gain insight into cloud characteristics. This document describes the finite cloud model and its verification for a stratus cloud

20 DISTRIBUTION/AVAILABILITY OF ABSTRACT ☐ UNCLASSIFIED/UNLIMITED ☒ SAME AS RPT ☐ DTIC USERS	21 ABSTRACT SECURITY CLASSIFICATION UNCLASSIFIED

22a. NAME OF RESPONSIBLE PERSON	22b TELEPHONE (include Area Code)	22c OFFICE SYMBOL
L. C. Russel	(619) 553-6132	Code 844

DD FORM 1473, 84 JAN

83 APR EDITION MAY BE USED UNTIL EXHAUSTED
ALL OTHER EDITIONS ARE OBSOLETE

UNCLASSIFIED

SECURITY CLASSIFICATION OF THIS PAGE

TABLE OF CONTENTS

LIST OF TABLES

LIST OF FIGURES

1.0 INTRODUCTION

Optical transmission through clouds is of importance in optical communications and remote sensing applications. In both downlink and uplink communications systems the transmission and reflection of signal and background light from clouds is of importance in determining the strength of the perceived signal-to-noise ratio. Of equal importance is the spatial, angular, and temporal spreading of the signal pulse in the cloud. That is, due to random scattering events in the cloud a collimated signal will be physically wider, decollimated, and arrive at the receiver over time periods exceeding the original pulse. All of these can impact the signal-to-noise ratio. Likewise, in remote sensing, a thorough understanding of the reflection from cloud surface is required in order to ascertain the cloud optical properties.

This report is part of an ongoing effort at NOSC to characterize clouds. In the past, most of the effort has been placed on the characterization of stratus clouds. In this connection, analytic models have been developed for cloud transmission and simulations have been carried out for spatial and temporal spreading. Now attention is being turned to finite clouds. The transmission and spreading (spatial, angular, and temporal) are all of interest for finite clouds.

A simulation was developed for radiative transfer in finite clouds in order to gain insight into the cloud characteristics. This report describes the finite cloud model and its verification for a stratus cloud. The results are compared with the current deterministic link models.

Section 2 contains a technical description of the model. Section 3 contains the results of cloud simulations and comparison with other models. Conclusions and recommendations are proffered in Section 4. References can be found in Section 5

2.0 TECHNICAL DISCUSSION

2.1 Background

The simulation of radiative transfer in clouds is carried out by the Monte Carlo method. In a Monte Carlo computation one photon at a time is followed in its three-dimensional path through a scattering medium. Its fate is determined by suitable probability distributions for mean free path, absorption, scattering angle, reflection angle from a surface, absorption at a surface and so on. The photon is followed until it is absorbed, detected, or leaves the field of interest. A sufficient number of such photons are followed until a picture of the system emerges. A detailed accounting of the Monte Carlo method is given in Appendix A.

Monte Carlo simulations have been used in the past at NOSC to develop models for spatial and temporal spreading in stratus clouds. These models consist of curve fits to simulation data and are necessarily limited in applicability to the ranges of optical and physical properties used in the simulations. The curve fits currently in use are not built upon analytic models and essentially have no physical basis. They have not been adequately documented and, as will be seen later, may not be applicable to communications problems.

For the treatment of finite clouds, a "cubic" (actually parallelpiped) cloud model has been developed. The model is supplemented by the intensity reference method which is used for the prediction of photon detection by surface receivers. In the following sections the cubic cloud model and intensity reference method are described. The application of these models to the prediction of signal, background, cloud transmission and optical thickness, and signal-to-noise ratio are described.

2.2 Cubic cloud model

The cubic cloud model consists of a parallelpiped cloud situated above the ground. The cloud geometry and coordinate system are shown in Figure 1. The three sides of the parallelpiped as well as the zenith and azimuth of the incoming photons may be specified independently. The model is then completely specified by the optical thickness of the cloud and the asymmetry parameter. The model uses the Henyey-Greenstein phase function for the prediction of scattering angle and Poisson statistics for the mean free path (see Appendix A for a more complete description.)

Photons may enter the cloud in from one to three faces, depending upon the source zenith and azimuth. For each face that receives photons a complete simulation is performed. Actually, these are identical calculations with the appropriate coordinate transformation and source angle. Moreover, the number of photons entering each face is adjusted so that each face has the same energy flux.

Thus, the model appropriately accounts for the photons entering different faces and computes the fraction of photons exiting from each of the six faces. In addition, the mean and standard deviation of the exit angle cosine, average position and distance traveled are computed. Table 1 shows a typical set of input and output.

In order to isolate the cloud behavior, the present cubic cloud model does not consider the surrounding atmosphere.

2.3 Intensity Reference Method

The cubic cloud model can be applied to communications problems by allowing the collection of photons at a receiver. Typically, the receiver is sufficiently far from the cloud and sufficiently small that literally millions of photons must be generated for each one reaching the receiver. Clearly, this is undesirable because of the large computation time required. Instead, recourse is made to an adaptation of the intensity reference method due to Meier, Lee, and Anderson (1978). In this technique, the probability of reaching the receiver is computed and stored as each photon exits the cloud. The accumulated probabilities are proportional to the intensity. A more detailed description of the intensity reference method is given in Appendix B.

The intensity reference method considers the probability of the photon reaching a detector as a consequence of a scattering event. Figure 2 shows a schematic of the method. Starting at the scattering event the photon has a probability of $P(\theta_s)d\omega$ of being scattered in the direction of the receiver (if it is in the receiver field of view). Along that path there may also be a probability of the photon being absorbed or scattered out of the path. In addition, if the photon is being multiply-scattered then a weighting function would also be applied if absorption is present.

The advantage of this method is that, in contrast to the low likelihood of a photon actually hitting receiver, there will always be some probability of it actually occurring. Thus, summing probabilities greatly improves the statistics, since each scattering event contributes to the intensity. In addition, the probability is computed exactly from the scattering point to the receiver; no other approximations are introduced. Moreover, the technique lends itself to vignetted receivers, i.e., receivers with a limited field of view (which lowers the likelihood of a photon hitting the receiver even further).

In the present adaptation of the intensity reference method the probability of reaching the receiver is computed as the photon exits the cloud. Thus, the photon is followed through the cloud until it exits, at which point the probability of being scattered toward the receiver is calculated from the last collision. More generally, the probabilities would be computed as the photon is scattered in the atmosphere.

A variation of the intensity reference method was tried assuming a Lambertian radiance profile at the cloud base. In this case, the probability is computed from the radiance profile rather than the scattering. The results so obtained were unsatisfactory because of inconsistencies with the global cloud transmission. This led to an investigation of the radiance profile beneath a cloud. These results showed that while the radiance profile beneath is a thick cloud is relatively independent of cloud optical thickness and source zenith it is not Lambertian. Rather, it is skewed

to favor forward scattered photons. These results are discussed in Section 3. At any rate, this method was not compatible with the intensity reference method.

The intensity reference method is well suited to this problem and would work equally well if there was an atmosphere. The success of the method is due largely to the far-field approximation being satisfied. Specifically, the receiver is small compared with the range and the solid angle may be considered as a differential. When this assumption breaks down the phase function must be integrated over the solid angle. This is discussed further in Appendix B.

2.4 Receivers

Two types of receivers were modeled to work in conjunction with the cubic cloud model. The first is a flat plate receiver with a cosine response function over a 90-degree half-angle field of view. The second is a vignetted receiver with a cosine response over a specified field of view (less than 90 degrees). These are referred to as "ideal" and "actual" receivers, respectively. They can also be thought of as representing radiometer and communications receivers, respectively. The results for the ideal receiver can be used to determine the cloud optical thickness from a simulation just as measured irradiance is used from a radiometer. The results for the actual receiver can be used to determine signal, background, and signal-to-noise ratio. These applications are discussed in the following sections.

2.5 Cloud Transmission Model

The method whereby cloud optical thickness can be inferred from a measured surface irradiance is well known (see, for example, Waldman, 1986). The optical thickness is expressed implicitly in the physical relationship between the perceived irradiance, cloud transmission, and source irradiance. In the simulation this translates to

$$\frac{x_b}{A_r} = \frac{N\mu_0}{A_c} L_c(\mu_0, \tau) \tag{1}$$

where x_b is the number of background photons reaching the receiver of area A_r from a source of N photons at a direction cosine μ_0 on a cloud of area A_c. The optical thickness τ can be obtained from Eq. (1) by iteration. L_c is the cloud transmission given by King and Harshvardhan (1986) and Waldman (1987). In developing Eq. (1) an ideal (flat plate) receiver has been assumed. The method applies equally well to a vignetted receiver if Eq. (1) is modified as follows

$$\frac{x_b}{A_r(1-\cos^2\theta)} = \frac{N\mu_0}{A_c} L_c(\mu_0,\tau) \tag{2}$$

where θ is the receiver field of view half-angle.

2.6 Signal-to-Noise Model

The signal-to-noise ratio is defined here as

$$S/N = \frac{n_s^2}{n_s + n_b} \tag{3}$$

where n_s and n_b are the number of signal of and background photoelectrons, respectively.

For a downlink these are defined as follows

$$n_s = E_s A_r f_{sg} \frac{\eta}{h\nu} T_r \tag{4}$$

$$n_b = P_b A_r f_{sg} B_f T \frac{\eta}{h\nu} T_r \tag{5}$$

Note that $E_s A_r f_{sg}$ in Eq. (4) is simply the fraction of signal energy reaching the receiver and $P_b A_r f_{sg}$ in Eq. (5) is the fraction of background power reaching the receiver. Equations (4) and (5) take the following form for a simulation

$$n_s = Q_0\left(\frac{x_s}{N}\right)\left(\frac{\eta}{h\nu}\right)T_r \tag{6}$$

$$n_b = E_0 \mu_0 A_c B_f T \left(\frac{x_b}{N}\right)\left(\frac{\eta}{h\nu}\right)T_r \tag{7}$$

where x_s and x_b are the signal and background photons collected in the simulation, respectively. Notice that, in general, these come from different simulations because the signal and background may have different zenith angles and spot sizes on top of the cloud (the background always covers the entire cloud, the signal spot may be any size).

Signal-to-noise ratio predictions from the simulations can be compared with those from a deterministic model. Such a model was developed for this purpose. It contains both signal and background calculations for a receiver below a stratus cloud. Spot shape is calculated so the results are sensitive to receiver position. There is no atmosphere in the model.

2.7 Pulsewidth Model

The receiver integration time, T is modeled as it is in the deterministic link model. For a matched filter it is usually taken as

$$T = 5t_m \approx 2t_{3dB} \tag{8}$$

Eq. (8) assumes a modified gamma function pulse; this may not generally be true. Appendix C contains a more detailed descirption of the modified gamma function.

The receiver integration time in this analysis was measured from the simulation pulse histogram.

3. RESULTS AND DISCUSSION

Several kinds of results were obtained in the course of testing and verifying the cubic cloud model. These are described below along with some typical results and their interpretation.

3.1 Simple cloud model

The cubic cloud model was tested on its own prior to applying it to the signal-to-noise calculation. The model should demonstrate symmetry and global energy conservation, and should give the same transmission as the deterministic model when the cloud length and width are much greater than height. The simulation was also tested to ensure that the results for a diffuse source agree with theoretical predictions; to wit, that a diffuse source produces the same result as an equivalent direction cosine of $\mu = 2/3$. The model does indeed satisfy all these criteria. Tables 1-3 shows the results for series of calculations in which the cloud is progressively increased in size while its thickness is held constant. These tables show that as the cloud area increases the photons exiting at the base approach the value of cloud transmission given by the deterministic model.

John Yen of NOSC has extended this cloud model to study the irradiance patterns on the surface beneath a finite cloud. His results will be reported separately.

3.2 Radiance Profiles

A simplified version of the cloud model was developed to study the radiance profiles upon reflection and transmission from a stratus cloud. The simplifications consist of removing the cloud edges (i.e., infinite cloud) and using a point source (rather than one distributed over the cloud area).

The program produces histograms of the transmission and reflection radiance profiles expressed as probability density functions versus angle. Figures 3-8 show comparisons of the reflection results with those for a Lambertian profile for two optical thicknesses (τ = 20 and 100) and three source zeniths (ζ=0°, 60° and diffuse). The results for the source at zenith (ζ=0°), i.e., Figs. 3 and 6 show non-Lambertian radiance which favors smaller angles, this effect being more pronounced at higher optical thickness. The results for an oblique source (ζ= 60°), i.e., Figs. 4 and 7, also exhibit a non-Lambertian radiance but here the larger angles are favored. Bear in mind, however, that these curves represent azimuthal averages and are not really representative of any particular directional reflectance function. The results for a diffuse source (assumed to be Lambertian) are shown in Figs. 5 and 8. For the smaller optical thickness (τ = 20) the result is similar to that for the oblique source. *For the larger optical thickness (τ = 100) the result is Lambertian.*

Figures 9-14 show comparisons of the transmission results with those for a Lambertian profile for the same conditions as above. These results are fairly uniform for all conditions. Specifically, all these cases demonstrate that the radiance profile is non-Lambertian and favor small angles; the radiance profiles are quite similar to each other. Figure 15 shows a composite plot of all the transmission histograms and comparison with a skewed-Lambertian profile. To first order, it can be concluded that the transmission radiance profile is independent of optical thickness and source zenith for thick clouds.

The skewed-Lambertian radiance profile can be represented by the probability density function

$$p(\theta) = (m+1)\cos^m\theta\sin\theta \tag{9}$$

or

$$p(\mu) = (m+1)\mu^m \tag{10}$$

where m = 1 for a Lambertian profile. A value of m = 1.552 (determined empirically) was used to generate the curve for Figure 15.

In summary, while conventional wisdom holds that the transmission and reflection functions are Lambertian, they are not. Transmission radiance profiles are always skewed to lower angles (i.e., they are more forward scattered than Lambertian) and reflection radiance profiles are sensitive to cloud optical thickness and source zenith. Only for reflection of diffuse light from very thick clouds (e.g., $\tau = 100$) was a Lambertian radiance profile observed.

3.3 Intensity Reference Method

The cloud model was extended to include a surface receiver on the ground. It was pointed out earlier that to actually collect photons at a small receiver is impractical and alternative methods were sought. The intensity reference method (IRM), described in Section 2.2 and Appendix B was implemented. Three probability models were examined. The first IRM model assumed that the radiance profile at the base of the cloud is Lambertian. In that case the probability of a photon being scattered to the receiver is

$$p = \frac{\mu}{\pi} d\,\omega \tag{11}$$

where $d\omega$ is the solid angle defined by the receiver from the photon exit point at the cloud base and μ is the direction cosine. The solid angle is written as a differential as a reminder that the analysis is valid for small solid angles. For larger solid angles the probability must be represented a an integral, viz.

$$p = \frac{1}{\pi}\int \mu d\,\omega \tag{12}$$

since the direction cosine cannot be regarded as a constant over the receiver area.

Table 4 shows the results of a computation with a Lambertian IRM model. The results are highly unsatisfactory insofar as the transmission predicted for the ideal receiver is 24% less than the actual value (as determined from the actual number of photons transmitted through the cloud). This discrepancy prompted the analysis of cloud radiance profiles discussed earlier in Section 3.2. It was concluded that the discrepancy was due in large part to the failure of the Lambertian radiance profile to adequately predict the forward-scattered nature of the radiance profile

The second IRM model assumed that the radiance profile at the base of the cloud is skewed-Lambertian (as described above). In that case the probability of a photon being scattered to the receiver is

$$p = \frac{m\mu^{m-1}}{2\pi} d\omega \tag{13}$$

Table 4 shows the results of the computation with the skewed-Lambertian IRM model. The results show considerable improvement with the error being brought down to 10%. This is better but not altogether satisfying. Recourse was made to a more detailed IRM calculation

In a formal sense the IRM should be based on the actual scattering events rather than on the global or macroscopic phenomena such as radiance profiles. Thus, the third IRM model made no assumptions about the radiance profile. Rather, when the photon is predicted to leave the cloud (i.e., its last scattering event), the probability of the photon reaching the receiver is determined by the scattering phase function, to wit,

$$p = P(\theta) d\omega \tag{14}$$

where $P(\theta)$ is the normalized phase function. The Henyey-Greenstein phase function used in this study is given by

$$P(\theta) = \frac{1}{4\pi} \frac{1 - g^2}{\left(1 + g^2 - 2g\mu\right)^{3/2}} \tag{15}$$

where g is the asymmetry parameter.

Table 4 shows the results of the computation with the Henyey-Greenstein IRM model. The error is about 2%. Clearly, this is the appropriate IRM model. Unfortunately, it is somewhat more computation intensive than the other methods because of the scattering geometry.

The Henyey-Greenstein IRM will be adopted for all further cloud and receiver simulation in this report.

3.4 RIMS Simulation/Inferred Optical Thickness

The Remote Irradiance Measuring Systems (RIMS) is a field unit for measuring irradiance. Optical thickness can be inferred from the measured irradiance. The cloud and receiver simulation are applicable to RIMS. To wit, the optical thickness can be inferred from "measured" (i.e., simulation) photons reaching the receiver. This method will be employed to determine the optical thickness in model calculations of signal-to-noise ratio.

3.5 Pulsewidth

The cubic cloud model was modified to record the temporal behavior of the photons. Specifically, as photons move through the cloud and to the receiver the times of transit are accumulated and the total transit time statistics are collected. Two types of statistics are developed. One is the simple mean and standard deviation while the other is a histogram of transit time.

Figures 16-21 show pulsewidth histograms for the ideal and actual receivers for a variety of conditions. Also shown for comparison is the Lee-Schroeder pulsewidth model (see, for example, Lee, et al. 1986). The latter model consists solely of a 3dB-pulsewidth calculation, but a modified gamma function is assumed for the pulse shape. Since Figs. 16-21 represent the same cloud optical and physical properties ($\tau = 20$, $Z = H = 1$ km) the model curve is the same in all the figures. These results show a considerable discrepancy between the present simulations and the model. The present results show a dependence of the pulsewidth on the signal spot size, receiver field of view, and receiver ground position which are unaccounted for by the model. Generally speaking, the model tends to overestimate the pulsewidth and the results get worse with diminishing receiver field of view.

Unfortunately, the model was never properly documented and so its origins are unknown. After some study and analysis it was concluded (i.e., guessed) that their model was based on a point source of photons and an infinite receiver (i.e., the time for any photons reaching the surface is counted). A simulation was run of the presumed model described above. The results and comparison with the model are shown in Figure 22. These results are in very good agreement with each other and with those shown in Lee, et al. (1986). This lends credence to the hypothesis of a point source and a distributed receiver and may explain why the model consistently overestimates the pulsewidth.

3.6 Signal-to-Noise Ratio Simulation

As described previously, the signal-to-noise ratio simulation must be developed from separate simulations for the signal and background. A suite of simulations was established for comparison with the link model. In all, twelve simulations were run including:

2 laser zenith angles,
2 laser spot sizes,
2 sun angles,
1 cloud condition, and
2 receiver locations.

Tables 5 through 16 show the results of the simulations. The analysis is limited to a single cloud condition ($\tau = 20$, $Z = H = 1$ km) because of the excessive computing time associated with the simulations. (Typically, three hours are required on a Compaq 386/20 with a Weitek coprocessor to get a decent pulse histogram.) Also, the receiver field of view half-angle was limited to 45°. Smaller field of view translates to longer computation time because fewer photons land in the field of view.

Looking at Tables 5-16 the following is observed: The user supplies the solar zenith, signal nadir, spot radius on the cloud, cloud top area, receiver displacement (along the x- or major-axis), the cloud thickness and height, and the receiver parameters used in the simulation. The user then provides the numbers of photons from the results of the background and signal simulations and the 3dB pulsewidth measured from the histograms (Figures 16-21). For the model, the spot extension must be specified. This was taken as approximately unity for a centered receiver and one-half for a receiver placed beneath the spot edge. The optical thickness for the downlink calculation is inferred from the background simulation. The results are shown in the lower part of the table. The 3dB pulsewidth, signal, background, and SNR are compared. Also, the receiver displacement (simulation) can be compared with (half of) the spot major axis on the surface (model).

Generally speaking the simulation and model signal predictions are in good agreement, with an average difference of about 1.1 dB. There are only two different background values, and they agree to within less than 0.5 dB. (These results would probably have been better if a larger cloud area was used, but that would have increased computation time). The signal-to-noise ratio for the simulation was typically 5 dB higher than that of the model. This is attributed in large part to the discrepancy of the simulation and model pulsewidth. Figure 23 shows a comparison of the signal-to-noise predictions for the simulation and model.

4.0 CONCLUSIONS AND RECOMMENDATIONS

A Monte Carlo simulation for finite parallelpiped clouds has been developed and tested for consistency with stratus (i.e., infinite) cloud models. Radiance profiles generated by the simulation were shown not to be Lambertian as is generally believed. On transmission, the radiance profiles appear to be relatively independent of source angle and optical thickness and exhibit a skewed radiance profile which favors smaller angles. On reflection, the radiance profiles cannot be so simply characterized. They are probably bidirectional (i.e., dependent upon the azimuth angle as well) and that was not considered in the present report. Only in the case of reflection of a diffuse (Lambertian) source off a very thick cloud was a Lambertian radiance profile observed.

Pulse histograms were generated for a number of source and receiver combinations for a given cloud condition. The pulsewidth and shape were found to be dependent upon the spot size, source zenith, and receiver field of view and surface location beneath the cloud in addition to its optical and physical properties. This is in sharp contrast with the model currently used in link programs which depends only upon the optical and physical properties. Simulated pulsewidths were of the order of one-half of the predicted values for the actual receiver.

Signal-to-noise ratios generated from simulations were also carried out and compared with model results. Generally, the background values agree well (less than 0.5 dB difference) and the signal values agree well (about 1 dB difference). But the signal-to-noise ratio is typically about 5 dB higher in the simulation than in the model, due in large part to the discrepancy in the pulsewidth.

The work described in this report shows that the cubic cloud model has great potential for expanding our understanding of radiative transfer in clouds. But this is only the first step. This model is a valid tool for studying non-uniform cloud optics and should be applied to the downlink, uplink, and remote sensing problems. Also, the results of the radiance profile and pulsewidth indicate that the spatial, angular and temporal spreading of light in stratus cloud should be re-examined.

5.0 REFERENCES

King, M.D. and Harshvardhan (1986). "Comparative Accuracy of the Albedo, Transmission, and Absorption for Selected Radiative Transfer Approximations," NASA Reference Publication 1160.

Lee, G., et al. (1986). "SLCAIR Report," Titan Systems, Inc.

Meier, R.R., Lee, J.-S., and Anderson, D.E. (1978). "Atmospheric Scattering of Middle UV Radiation from an Internal Source," Appl. Optics, 17, No. 20, pp 3216-3225.

Waldman, C.H. (1986). "Optical Thickness Prediction from Measured Background Irradiance," report prepared for Titan Systems, Inc.

Waldman, C.H. (1987). "Optical Transmission Through Clouds by Direct and Diffuse Radiation," report prepared for Titan Systems, Inc.

```
S I M U L A T I O N   O F   L I G H T   S C A T T E R I N G   I N   C L O U D S
                              SVS/Weitek Version
Select C                          IRS Model                             ^Print OFF
--------------------------------------------------------------------------------

N(o. of photons...............   25000    X( dimension (km).............   1.00
                                          Y( dimension (km).............   1.00
S(ource zenith (deg)..........   30.00    Z( dimension (km).............   1.00
A(zimuth (deg)................   30.00
                                          Estimated time................  12.50
O(ptical thickness of cloud...   50.00    Start time................11:21:34.55
g( asymmetry param for scat...   0.875    End time..................11:29:12.79
Continuum model Lc............   17.42
```

	X+	Y+	Z+	X-	Y-	Z-
count (%)	13.24	13.33	10.01	20.89	18.21	24.32
<cos>	0.667	0.662	0.749	-0.642	-0.622	-0.675
dev	0.374	0.388	0.412	0.380	0.388	0.375
X	0.500	-0.082	-0.206	-0.500	-0.021	0.001
Y	-0.040	0.500	-0.113	-0.004	-0.500	0.003
Z	-0.231	-0.185	0.500	-0.038	-0.065	-0.500
<d>	0.709	0.736	0.712	0.602	0.614	0.635

```
C:\TP\NOSC\CLOUD>
```

Table 1. Results of Cubic Cloud Simulation (1x1x1 km Cloud)

S I M U L A T I O N   O F   L I G H T   S C A T T E R I N G   I N   C L O U D S

SVS/Weitek Version

Select C	IRS Model	^Print OFF

N(o. of photons...............	25000	X(dimension (km).............	5.00
		Y(dimension (km).............	5.00
S(ource zenith (deg)..........	30.00	Z(dimension (km).............	1.00
A(zimuth (deg)................	30.00		
		Estimated time................	12.50
O(ptical thickness of cloud...	50.00	Start time................	12:03:01.63
g(asymmetry param for scat...	0.875	End time..................	12:15:20.60
Continuum model Lc.......... .	17.42		

	X+	Y+	Z+	X-	Y-	Z-
count (%)	4.90	4.47	15.27	8.32	6.90	60.14
<cos>	0.681	0.674	0.718	-0.659	-0.643	-0.682
dev	1.421	1.438	1.971	1.424	1.406	1.946
X	2.500	-0.113	-0.344	-2.500	-0.015	-0.015
Y	-0.080	2.500	-0.166	-0.044	-2.500	-0.014
Z	-0.235	-0.210	0.500	-0.050	-0.072	-0.500
<d>	1.258	1.421	3.514	1.048	1.082	1.410

C:\TP\NCSC\CLOUD>

Table 2. Results of Cubic Cloud Simulation (5x5x1 km Cloud)

```
S I M U L A T I O N   O F   L I G H T   S C A T T E R I N G   I N   C L O U D S
                              SVS/Weitek Version
Select C                          IRS Model                            ^Print OFF
--------------------------------------------------------------------------------

N(o. of photons..............   25000    X( dimension (km)............   10.00
                                         Y( dimension (km)............   10.00
S(ource zenith (deg)..........  30.00    Z( dimension (km)............    1.00
A(zimuth (deg)................  30.00
                                         Estimated time...............   12.50
O(ptical thickness of cloud...  50.00    Start time.................12:16:30.85
g( asymmetry param for scat...  0.875    End time...................12:29:54.74
Continuum model Lc............  17.42
```

	X+	Y+	Z+	X-	Y-	Z-
count (%)	2.70	2.46	17.52	4.53	3.82	68.98
<cos>	0.679	0.696	0.712	-0.654	-0.623	-0.682
dev	2.830	2.837	3.979	2.863	2.829	3.970
X	5.000	-0.162	-0.339	-5.000	0.051	-0.028
Y	-0.128	5.000	-0.172	0.062	-5.000	-0.021
Z	-0.212	-0.211	0.500	-0.041	-0.074	-0.500
<d>	1.498	1.532	4.040	1.081	1.143	1.562

```
C:\TP\NCST\CLOUD>
```

Table 3. Results of Cubic Cloud Simulation (10x10x1 km Cloud)

PERCENT TRANSMISSION CALCULATED WITH IRM

Model	Lambertian Radiance Profile	Skewed-Lambertian Radiance Profile	Henyey-Greenstein Scattering Function
Total trans thru cloud	32.63	32.63	32.63
Predicted by model	24.80	29.33	33.30
Percent difference	-24.00	-10.10	+2.05

Table 4. Comparison of Cloud Transmission from Intensity Reference Models

```
C O M P A R I S O N   O F   S I M U L A T I O N  w/  D O W N L I N K   M O D E L
                                Simple Cloud Model
Select @                         Turbo Pascal 5.0                        ^Print  ON
-----------------------------------------------------------------------------------
Z(enith of sun (deg).........     0.00
N(adir of signal (deg).......     0.00
S(pot equiv rad on cloud (km).    5.64
C(loud area (km^2)...........   100.00

P(hotons: total signal.......  5.000E5
          rec'd signal....... 9.227E-4   Optical thickness............    24.70
          total bkgnd........  5.000E5   T(hickness of cloud (km).....     1.00
          rec'd bkgnd........ 9.227E-4   H(eight of cloud (km)........     1.00
          ideal bkgnd........ 1.651E-3   eX(tension of spot from max...    0.999

          S I M U L A T I O N                      L I N K   M O D E L
-----------------------------------------------------------------------------------
D(isplacement of rec'r (km)...    0.00   Spot major axis on surf (km)..     1.84
t3(dB (usec).................     3.75   t3dB (usec)..................     9.92
Signal (dB Joules)...........   -84.33   Signal (dB Joules)...........   -85.03
Background (dB W/m^2/nm).....    -1.32   Background (dB W/m^2/nm).....    -1.80
SNR (dB).....................    70.80   SNR (dB).....................    65.84
```

Table 5. Comparison of Simulation and Model Signal, Background, and S/N

```
C O M P A R I S O N   O F   S I M U L A T I O N  w/  D O W N L I N K   M O D E L
                            Simple Cloud Model
Select @                     Turbo Pascal 5.0                          ^Print ON
--------------------------------------------------------------------------------
Z enith of sun (deg)..........    0.00
N adir of signal (deg)........   60.00
S pot equiv rad on cloud (km).    5.64
C loud area (km^2)............  100.00

P hotons: total signal........  5.000E5
          rec'd signal... .... 6.015E-4   Opt cal thickness............   24.70
          total bkgnd... .....  5.000E5   T hickness of cloud (km)... ..    1.00
          rec'd bkgnd......... 9.027E-4   H eight of cloud (km).........    1.00
          ideal bkgnd......... 1.651E-3   eX tension of spot from max...   0.999

          S I M U L A T I O N                       L I N K   M O D E L
--------------------------------------------------------------------------------
D isplacement of rec'r (km). .    0.00   Spot major axis on surf (km)..    5.18
t3 dB (usec)..................    6.04   t3dB (usec)...................    9.92
Signal (dB Joules)............  -86.19   Signal (dB Joules)............  -86.68
Background (dB W/m^2/nm)......   -1.32   Background (dB W/m^2/nm)......   -1.80
SNR (dB.......................   65.18   SNR (dB)......................   62.57
```

Table 6. Comparison of Simulation and Model Signal, Background, and S/N

```
C O M P A R I S O N   O F   S I M U L A T I O N  w/  D O W N L I N K   M O D E L
                               Simple Cloud Model
Select @                        Turbo Pascal 5.0                        ^Print  ON
---------------------------------------------------------------------------------
Z(enith of sun (deg)..........    0.00
N(adir of signal (deg)........    0.00
S(pot equiv rad on cloud (km).    2.00
C(loud area (km^2)............  100.00

P(hotons: total signal........  7.500E5
          rec'd signal........ 9.796E-3  Optical thickness.............   24.70
          total bkgnd.........  5.000E5  T(hickness of cloud (km)......    1.00
          rec'd bkgnd......... 9.227E-4  H(eight of cloud (km).........    1.00
          ideal bkgnd......... 1.651E-3  eX(tension of spot from max...   0.999

          S I M U L A T I O N                    L I N K   M O D E L
---------------------------------------------------------------------------------
D(isplacement of rec'r (km)...     0.00  Spot major axis on surf (km)..    0.23
t3(dB (usec)..................     4.38  t3dB (usec)...................    9.92
Signal (dB Joules)............   -75.83  Signal (dB Joules)............  -77.58
Background (dB W/m^2/nm)......    -1.32  Background (dB W/m^2/nm)......   -1.80
SNR (dB)......................    85.93  SNR (dB)......................   80.29
```

Table 7. Comparison of Simulation and Model Signal, Background, and S/N

```
C O M P A R I S O N   O F   S I M U L A T I O N  W/  D O W N L I N K   M O D E L
                             Simple Cloud Model
Select 3                     Turbo Pascal 5.0                            ^Print  ON
-----------------------------------------------------------------------------------
Z(enith of sun (deg)..........    0.00  R(eceiver Area (m^2)..........
N(adir of signal (deg)........    0.00    Bandwidth (nm)..............
S(pot equiv rad on cloud (km).    2.00    Transmission................
C(loud area (km^2)............  100.00    Quantum efficiency..........
                                          FOV (+/- deg)...............
P(hotons: total signal........ 9.000E5
          rec'd signal........ 5.268E-3 Optical thickness.............  24.70
          total bkgnd......... 5.000E5  T(hickness of cloud (km)......   1.00
          rec'd bkgnd......... 9.227E-4 H(eight of cloud (km).........   1.00
          ideal bkgnd......... 1.651E-3 eX(tension of spot from max...  0.500

          S I M U L A T I O N                    L I N K   M O D E L
-----------------------------------------------------------------------------------
D(isplacement of rec'r (km)...    2.00  Spot major axis on surf (km)..   4.17
t3 dB (usec)..................    3.96  t3dB (usec)...................   3.32
Signal (dB Joules)............  -79.32  Signal (dB Joules)............ -80.59
Background (dB W/m^2/nm)......   -1.32  Background (dB W/m^2/nm)......  -1.80
SNR (dB ......................   80.08  SNR (dB)......................  74.54
```

Table 8. Comparison of Simulation and Model Signal, Background, and S/N

```
C O M P A R I S O N   O F   S I M U L A T I O N  w/  D O W N L I N K   M O D E L
                              Simple Cloud Model
Select 3                       Turbo Pascal 5.0                             ^Print ON
-------------------------------------------------------------------------------------
Z(enith of sun (deg)..........   0.00   R(eceiver Area (m^2)..........
N(adir of signal (deg)........  60.00     Bandwidth (nm)..............
S(pot equiv rad on cloud (km).   2.00     Transmission................
C(loud area (km^2)............ 100.00     Quantum efficiency..........
                                          FOV (+/- deg).............. .
P(hotons: total signal........ 9.000E5
          rec'd signal........ 7.624E-3  Optical thickness.............   24.70
          total bkgnd......... 5.000E5   T(hickness of cloud (km)......    1.00
          rec'd bkgnd......... 9.227E-4  H(eight of cloud (km).........    1.00
          ideal bkgnd......... 1.651E-3  eX(tension of spot from max...    0.999

          S I M U L A T I O N                      L I N K   M O D E L
-------------------------------------------------------------------------------------
D(isplacement of rec'r (km)...   0.00   Spot major axis on surf (km)..    0.38
t3(dB (usec)..................   5.00   t3dB (usec)...................    9.92
Signal (dB Joules)............ -77.71   Signal (dB Joules)............  -79.23
Background (dB W/m^2/nm)......  -1.32   Background (dB W/m^2/nm)......   -1.80
SNR (dB)......................  82.17   SNR (dB)......................   77.15
```

Table 9. Comparison of Simulation and Model Signal, Background, and S/N

```
C O M P A R I S O N   O F   S I M U L A T I O N  w/  D O W N L I N K   M O D E L
                              Simple Cloud Model
Select @                       Turbo Pascal 5.0                          ^Print  ON
-----------------------------------------------------------------------------------
Z(enith of sun (deg)..........    0.00   R(eceiver Area (m^2)..........
N(adir of signal (deg)........   60.00     Bandwidth (nm)..............
S(pot equiv rad on cloud (km).    2.00     Transmission................
C(loud area (km^2)............  100.00     Quantum efficiency..........
                                           FOV (+/- deg)...............
P(hotons: total signal........ 9.000E5
          rec'd signal........ 3.641E-3  Optical thickness.............   24.70
          total bkgnd......... 5.000E5   T(hickness of cloud (km)......    1.00
          rec'd bkgnd......... 9.227E-4  H(eight of cloud (km).........    1.00
          ideal bkgnd......... 1.651E-3  eX(tension of spot from max...   0.500

          S I M U L A T I O N                      L I N K   M O D E L
-----------------------------------------------------------------------------------
D(isplacement of rec'r (km)...    2.83   Spot major axis on surf (km)..    5.73
t3(dB (usec)..................    4.79   t3dB (usec)...................    9.92
Signal (dB Joules)............  -80.92   Signal (dB Joules)............  -82.24
Background (dB W/m^2/nm)......   -1.32   Background (dB W/m^2/nm)......   -1.80
SNR (dB)......................   76.36   SNR (dB)......................   71.32
```

Table 10. Comparison of Simulation and Model Signal, Background, and S/N

```
C O M P A R I S O N   O F   S I M U L A T I O N  w/  D O W N L I N K   M O D E L
                              Simple Cloud Model
Select @                      Turbo Pascal 5.0                        ^Print  ON
---------------------------------------------------------------------------------
Z(enith of sun (deg)..........   60.00  R(eceiver Area (m^2)..........
N(adir of signal (deg)........    0.00    Bandwidth (nm)..............
S(pot equiv rad on cloud (km).    5.64    Transmission................
C(loud area (km^2)............  100.00    Quantum efficiency..........
                                          FOV (+/- deg)...............
P(hotons: total signal........ 5.000E5
          rec'd signal........ 9.227E-4  Optical thickness.............   25.72
          total bkgnd......... 5.000E5   T(hickness of cloud (km)......    1.00
          rec'd bkgnd......... 6.015E-4  H(eight of cloud (km).........    1.00
          ideal bkgnd......... 1.096E-3  eX(tension of spot from ma.....  0.999

          S I M U L A T I O N                  L I N K   M O D E L
---------------------------------------------------------------------------------
D(isplacement of rec'r (km)...    0.00  Spot major axis on surf (km)..    1.85
t3(dB (usec)......   ........     3.75  t3dB (usec)...................   10.17
Signal (dB Joules)............  -84.33  Signal (dB Joules)............  -85.15
Background (dB W/m^2/nm)......   -6.19  Background (dB W/m^2/nm)......   -6.59
SNR (dB)......................   75.14  SNR (dB)......................   70.08
```

Table 11. Comparison of Simulation and Model Signal, Background, and S/N

C O M P A R I S O N   O F   S I M U L A T I O N w/ D O W N L I N K   M O D E L

Simple Cloud Model

Select @ — Turbo Pascal 5.0 — ^Print ON

Z(enith of sun (deg)..........	60.00	R(eceiver Area (m^2)..........	
N(adir of signal (deg)........	60.00	Bandwidth (nm)..............	
S(pot equiv rad on cloud (km).	5.64	Transmission................	
C(loud area (km^2)...........	100.00	Quantum efficiency..........	
		FOV (+/- deg)...............	
P(hotons: total signal........	5.000E5		
rec'd signal........	6.015E-4	Optical thickness.............	25.72
total bkgnd.........	5.000E5	T(hickness of cloud (km)......	1.00
rec'd bkgnd.........	6.015E-4	H(eight of cloud (km).........	1.00
ideal bkgnd.........	1.096E-3	eX(tension of spot from max...	0.999

S I M U L A T I O N		L I N K M O D E L	
D(isplacement of rec'r (km)...	0.00	Spot major axis on surf (km)..	5.21
t3(dB (usec)..................	6.04	t3dB (usec)...................	10.17
Signal (dB Joules)............	-86.19	Signal (dB Joules)............	-86.81
Background (dB W/m^2/nm)......	-6.19	Background (dB W/m^2/nm)......	-6.59
SNR (dB)......................	69.82	SNR (dB)......................	66.87

Table 12. Comparison of Simulation and Model Signal, Background, and S/N

```
C O M P A R I S O N   O F   S I M U L A T I O N  w/  D O W N L I N K   M O D E L
                              Simple Cloud Model
Select @                      Turbo Pascal 5.0                          ^Print  ON
-----------------------------------------------------------------------------------
Z(enith of sun (deg)..........   60.00  R(eceiver Area (m^2)..........
N(adir of signal (deg)........    0.00    Bandwidth (nm)..............
S(pot equiv rad on cloud (km).    2.00    Transmission..............
C(loud area (km^2)............  100.00    Quantum efficiency..........
                                          FOV (+/- deg)...............
P(hotons: total signal........ 7.500E5
          rec'd signal........ 9.796E-3  Optical thickness.............   25.72
          total bkgnd......... 5.000E5   T(hickness of cloud (km)......    1.00
          rec'd bkgnd......... 6.015E-4  H(eight of cloud (km).........    1.30
          ideal bkgnd......... 1.096E-3  eX(tension of spot from max...   0.999

          S I M U L A T I O N                      L I N K   M O D E L
-----------------------------------------------------------------------------------
D(isplacement of rec'r (km)...    0.00  Spot major axis on surf (km)..    0.23
t3(dB (usec)..................    4.38  t3dB (usec)...................   10.17
Signal (dB Joules)............  -75.83  Signal (dB Joules)............  -77.70
Background (dB W/m^2/nm)......   -6.19  Background (dB W/m^2/nm)......   -6.59
SNR (dB)......................   88.77  SNR (dB)......................   83.87
```

Table 13. Comparison of Simulation and Model Signal, Background, and S/N

```
C O M P A R I S O N   O F   S I M U L A T I O N  w/  D O W N L I N K   M O D E L
                              Simple Cloud Model
Select @                       Turbo Pascal 5.0                          ^Print  ON
-----------------------------------------------------------------------------------
Z(enith of sun (deg)..........   60.00  R(eceiver Area (m^2)..........
N(adir of signal (deg)........    0.00    Bandwidth (nm)..............
S(pot equiv rad on cloud (km).    2.00    Transmission................
C(loud area (km^2)............  100.00    Quantum efficiency..........
                                          FOV (+/- deg)...............
P(hotons: total signal........ 9.000E5
          rec'd signal........ 5.268E-3  Optical thickness.............   25.72
          total bkgnd......... 5.000E5   T(hickness of cloud (km)......    1.00
          rec'd bkgnd......... 6.015E-4  H(eight of cloud (km).........    1.00
          ideal bkgnd......... 1.096E-3  eX(tension of spot from max...   0.500

          S I M U L A T I O N                     L I N K   M O D E L
-----------------------------------------------------------------------------------
D(isplacement of rec'r (km)...    2.00  Spot major axis on surf (km)..    4.17
t3(dB (usec)..................    3.96  t3dB (usec)...................   10.17
Signal (dB Joules)............  -79.32  Signal (dB Joules)............  -80.71
Background (dB W/m^2/nm)......   -6.19  Background (dB W/m^2/nm)......   -6.59
SNR (dB)......................   83.66  SNR (dB)......................   78.51
```

Table 14. Comparison of Simulation and Model Signal, Background, and S/N

```
C O M P A R I S O N   O F   S I M U L A T I O N  w/  D O W N L I N K   M O D E L
                              Simple Cloud Model
Select @                      Turbo Pascal 5.0                          ^Print  ON
----------------------------------------------------------------------------------
Z(enith of sun (deg)..........    60.00   R(eceiver Area (m^2).........
N(adir of signal (deg)........    60.00     Bandwidth (nm)..............
S(pot equiv rad on cloud (km)      2.00     Transmission................
C(loud area (km^2)............   100.00     Quantum efficiency..........
                                            FOV (+/- deg)...............
P(hotons: total signal........  9.000E5
          rec'd signal........ 7.624E-3   Optical thickness.............   25.72
          total bkgnd.........  5.000E5   T(hickness of cloud (km)......    1.00
          rec'd bkgnd......... 6.015E-4   H(eight of cloud (km).........    1.00
          ideal bkgnd......... 1.096E-3   eX(tension of spot from max...   0.999

          S I M U L A T I O N                    L I N K   M O D E L
----------------------------------------------------------------------------------
D(isplacement of rec'r (km)...     0.00   Spot major axis on surf (km)..    0.38
t3(dB (usec)..................     5.00   t3dB (usec)...................   10.17
Signal (dB Joules)............   -77.71   Signal (dB Joules)............  -79.35
Background (dB W/m^2/nm)......    -6.19   Background (dB W/m^2/nm)......   -6.59
SNR (dB)......................    85.62   SNR (dB)......................   80.97
```

Table 15. Comparison of Simulation and Model Signal, Background, and S/N

```
C O M P A R I S O N   O F   S I M U L A T I O N  w/  D O W N L I N K   M O D E L
                               Simple Cloud Model
Select @                       Turbo Pascal 5.0                          ^Print  ON
-------------------------------------------------------------------------------------
Z(enith of sun (deg)..........   60.00  R(eceiver Area (m^2)..........
N(adir of signal (deg)........   60.00    Bandwidth (nm)..............
S(pot equiv rad on cloud (km).    2.00    Transmission................
C(loud area (km^2)............  100.00    Quantum efficiency..........
                                          FOV (+/- deg)...............
P(hotons: total signal........ 9.000E5
          rec'd signal........ 3.641E-3  Optical thickness.........  ....   25.72
          total bkgnd......... 5.000E5   T(hickness of cloud (km)......      1.00
          rec'd bkgnd......... 6.015E-4  H(eight of cloud (km).........      1.00
          ideal bkgnd......... 1.096E-3  eX(tension of spot from max...     0.500

          S I M U L A T I O N                      L I N K   M O D E L
-------------------------------------------------------------------------------------
D(isplacement of rec'r (km)...    2.83  Spot major axis on surf (km)..      5.73
t3(dB (usec)..................    4.79  t3dB (usec)...................     10.17
Signal (dB Joules)............  -80.92  Signal (dB Joules)............    -82.36
Background (dB W/m^2/nm)......   -6.19  Background (dB W/m^2/nm)......     -6.59
SNR (dB)......................   80.40  SNR (dB)......................     75.43
```

Table 16. Comparison of Simulation and Model Signal, Background, and S/N

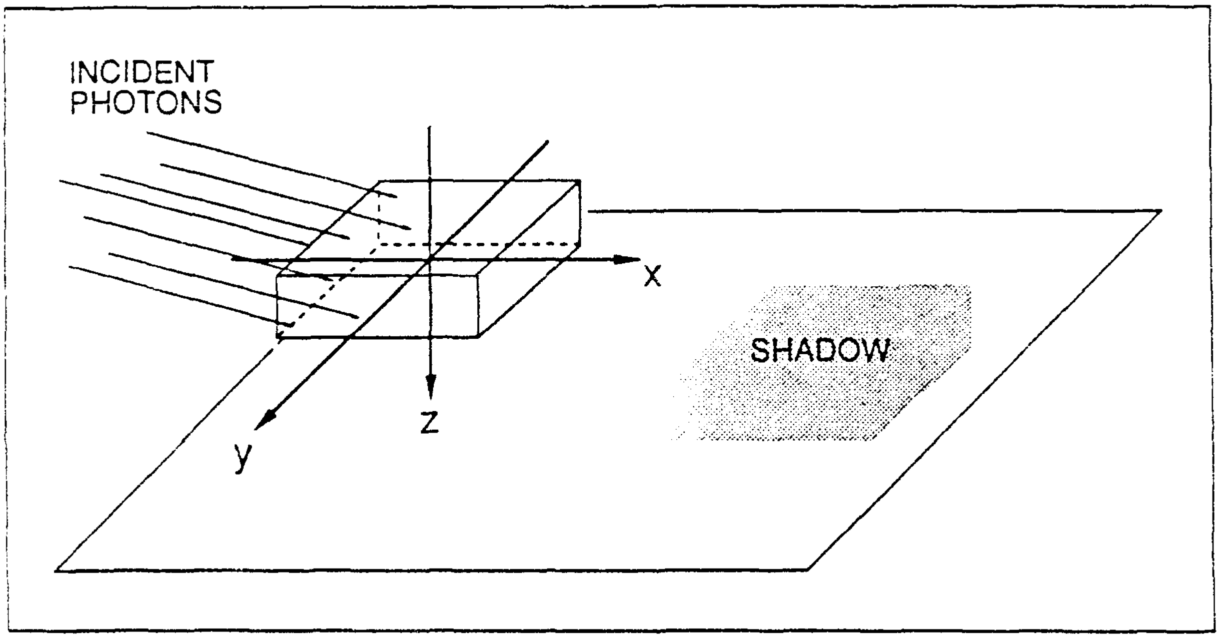

Figure 1. Schematic Drawing of Cubic Cloud Model

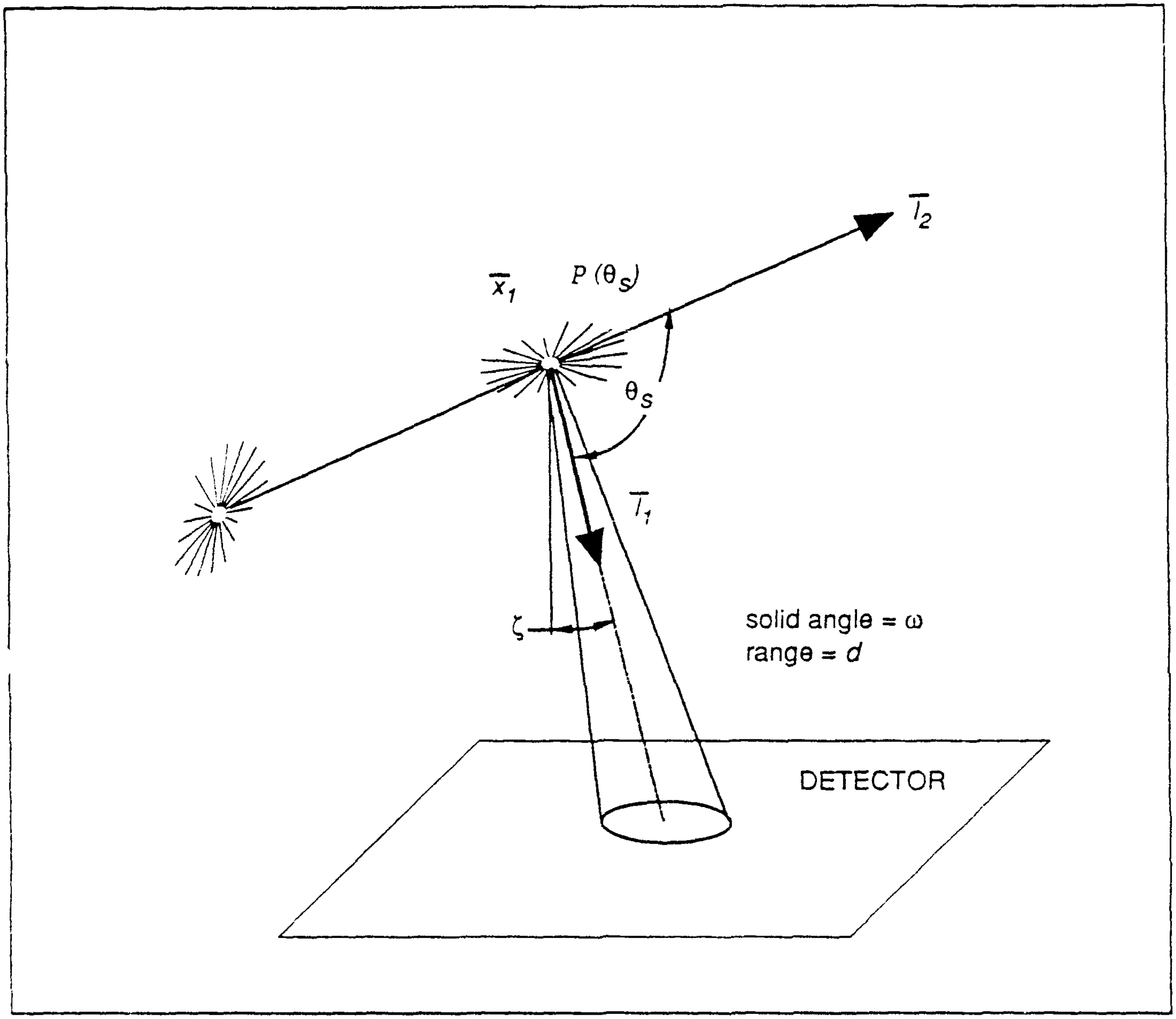

Figure 2. Schematic of Intensity Reference Method

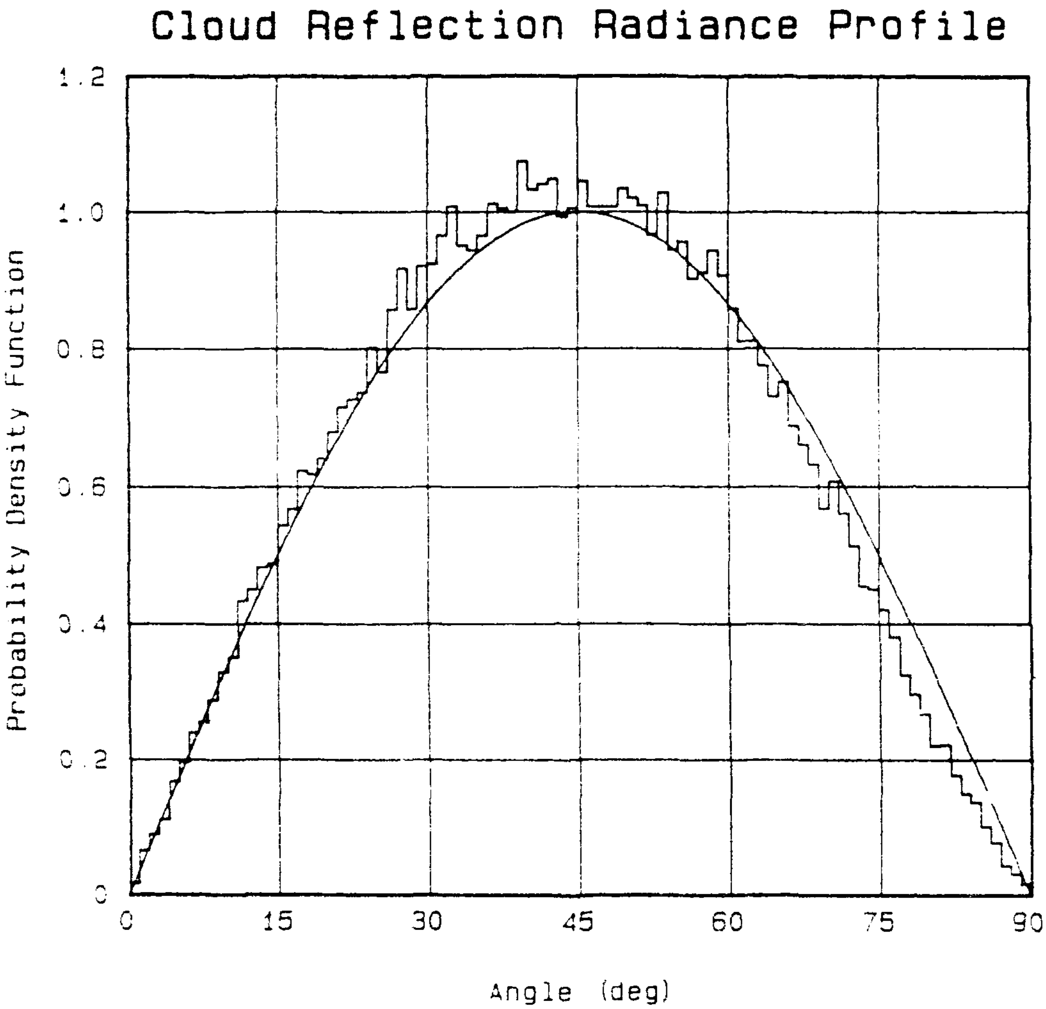

Simulation vs. Lambertian

Tau = 20
Zenith = 0
100,000 Random Trials

Figure 3 Comparison of Simulation and Lambertian Radiance Profile (Cloud Reflection)

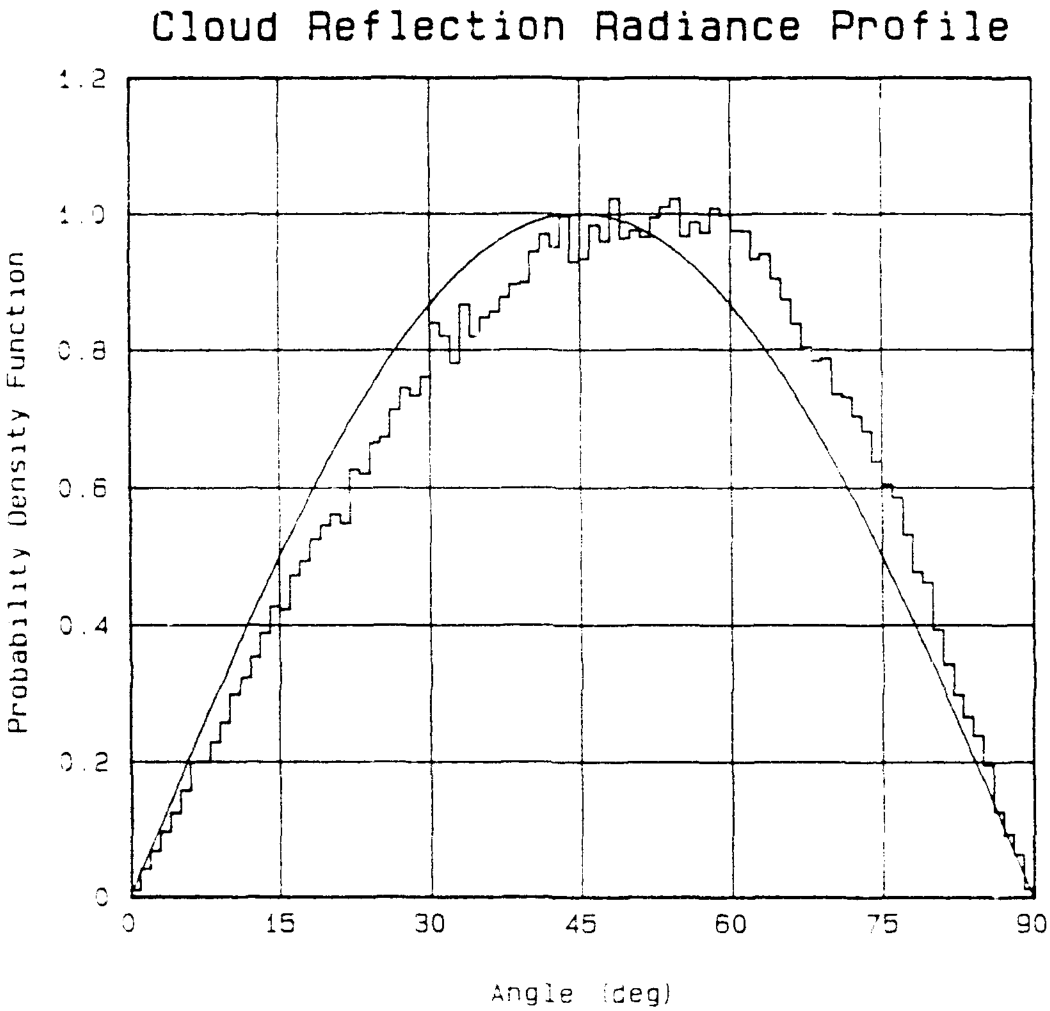

Simulation vs. Lambertian

Tau = 20
Zenith = 60
100,000 Random Trials

Figure 4. Comparison of Simulation and Lambertian Radiance Profile (Cloud Reflection)

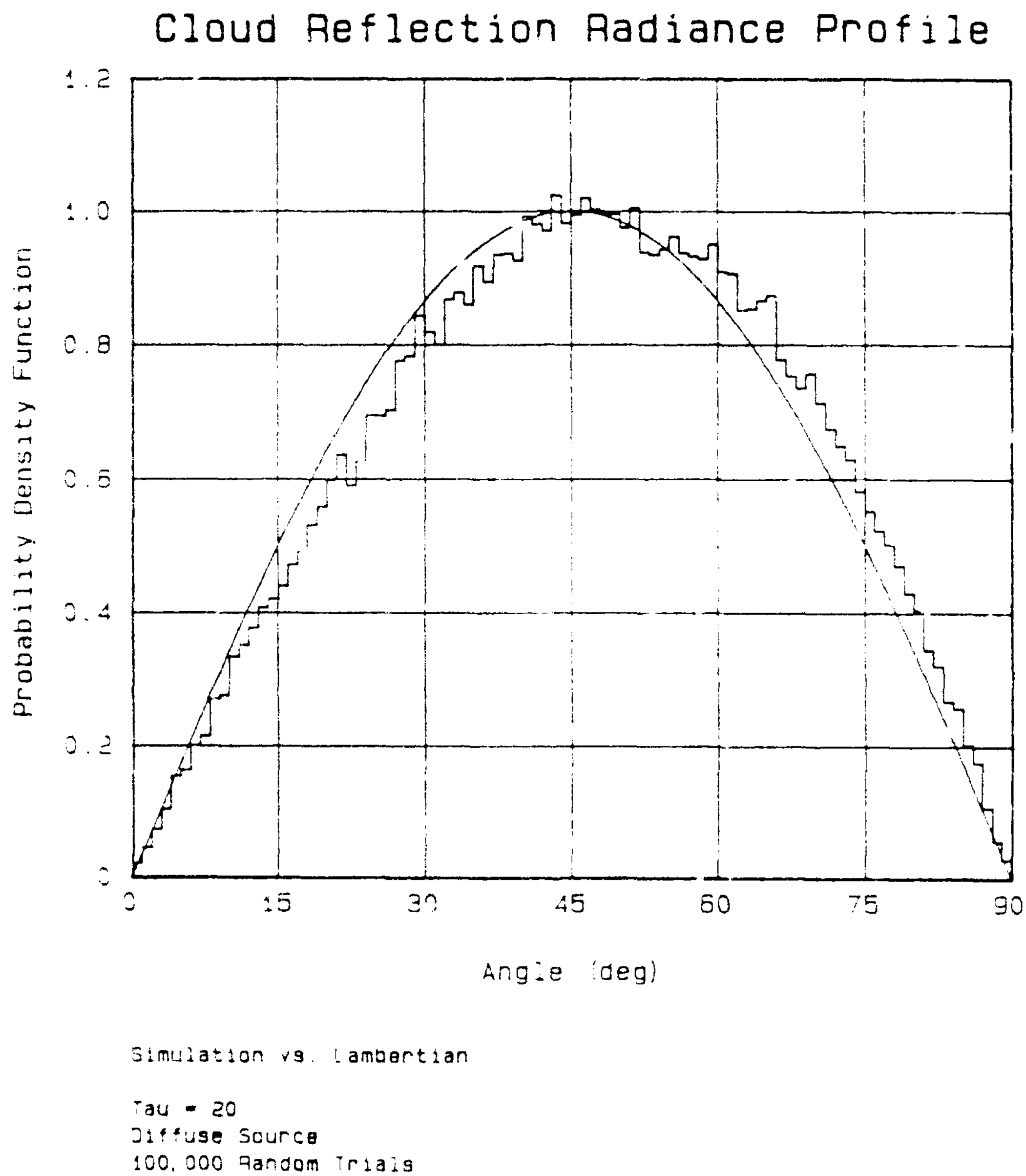

Figure 5. Comparison of Simulation and Lambertian Radiance Profile
(Cloud Reflection)

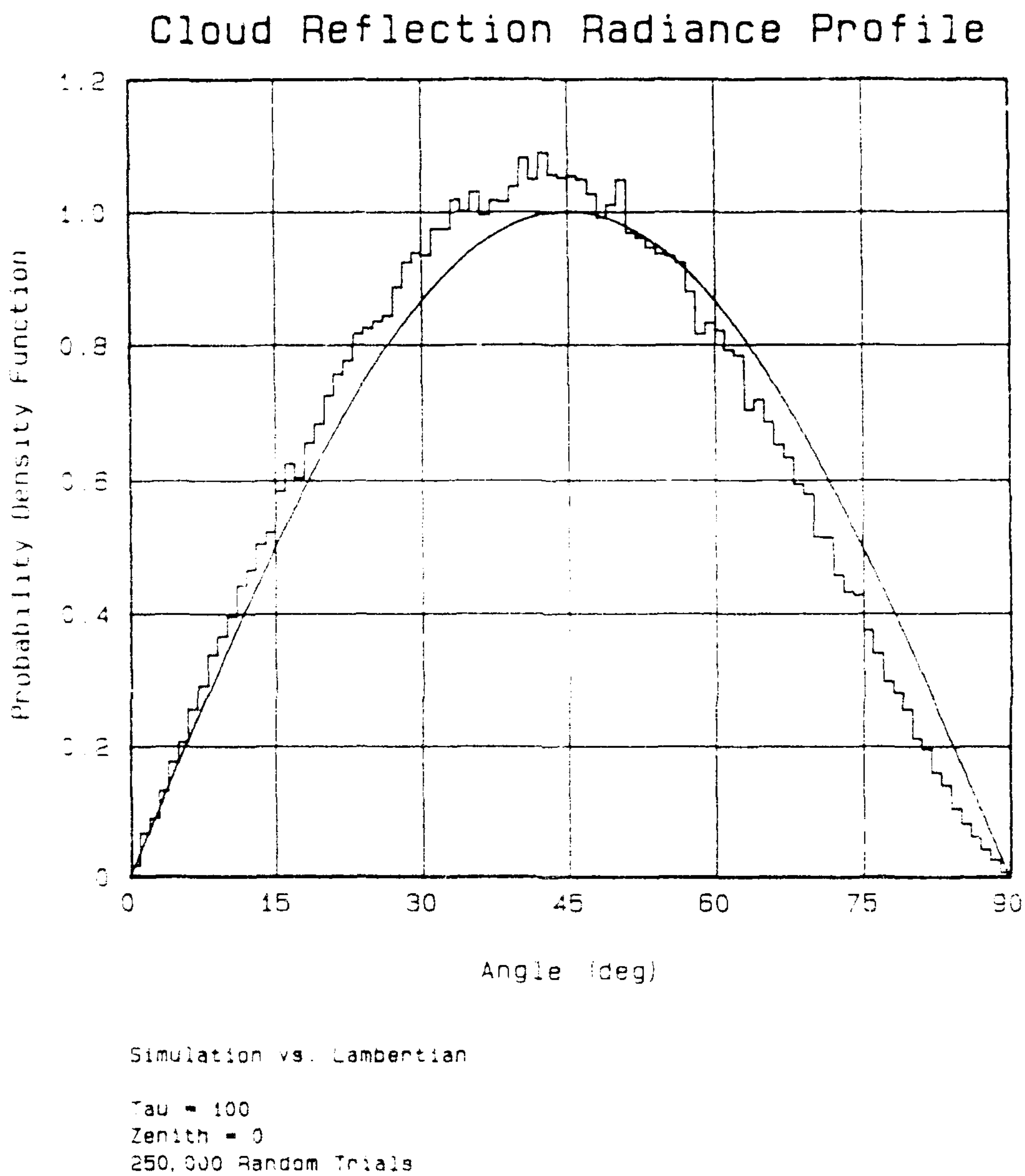

Figure 6. Comparison of Simulation and Lambertian Radiance Profile (Cloud Reflection)

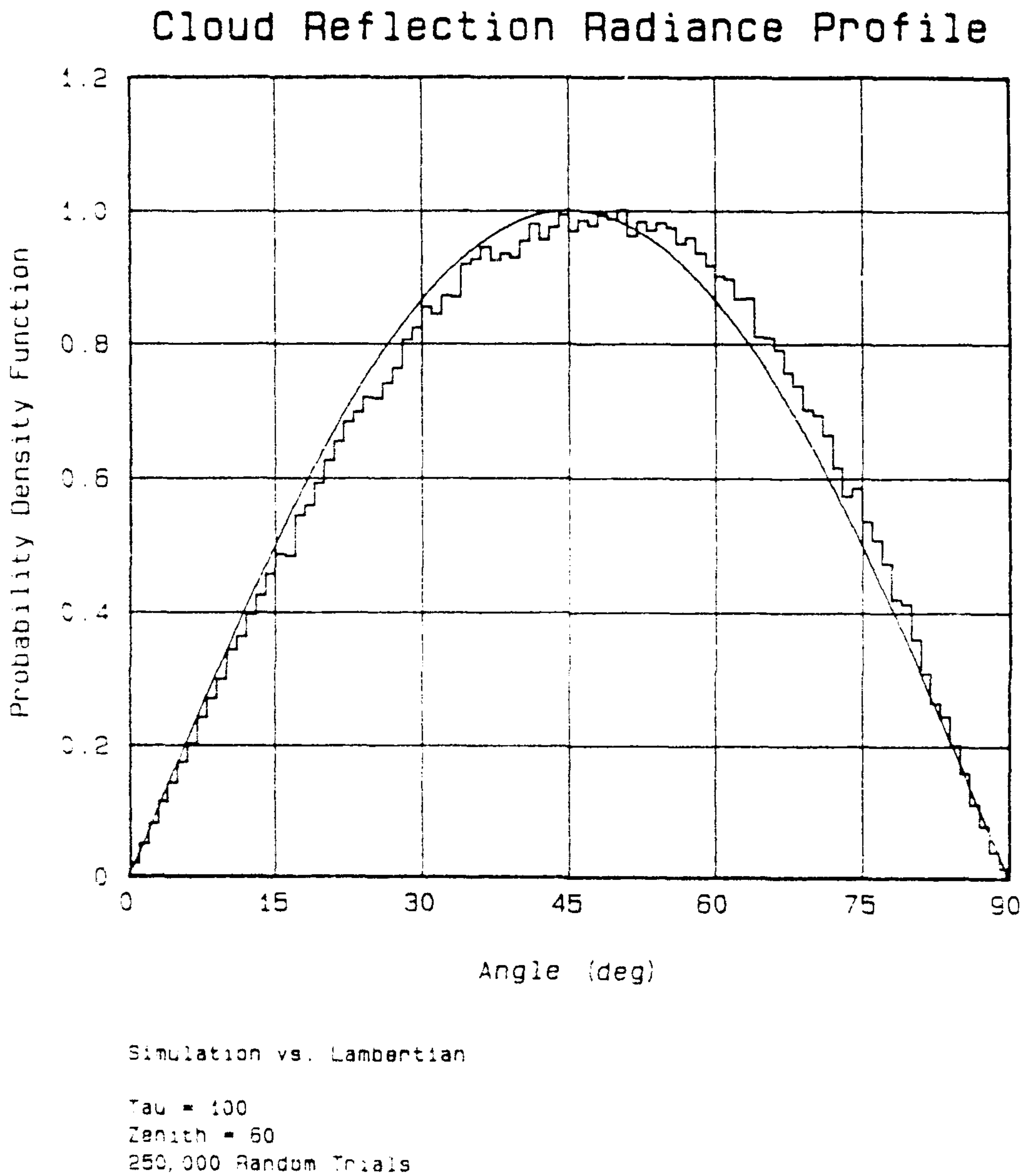

Figure 7. Comparison of Simulation and Lambertian Radiance Profile
(Cloud Reflection)

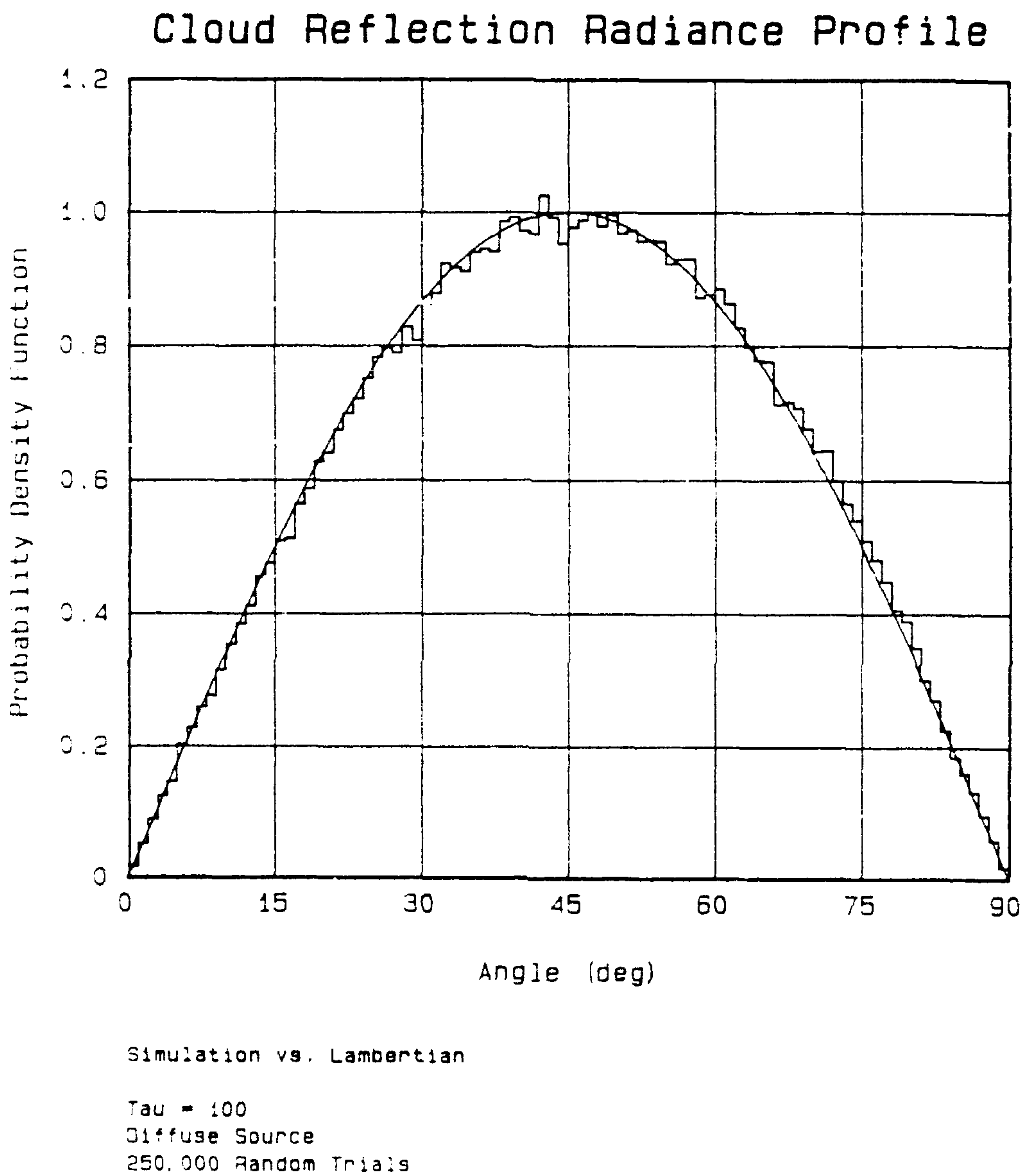

Figure 8. Comparison of Simulation and Lambertian Radiance Profile (Cloud Reflection)

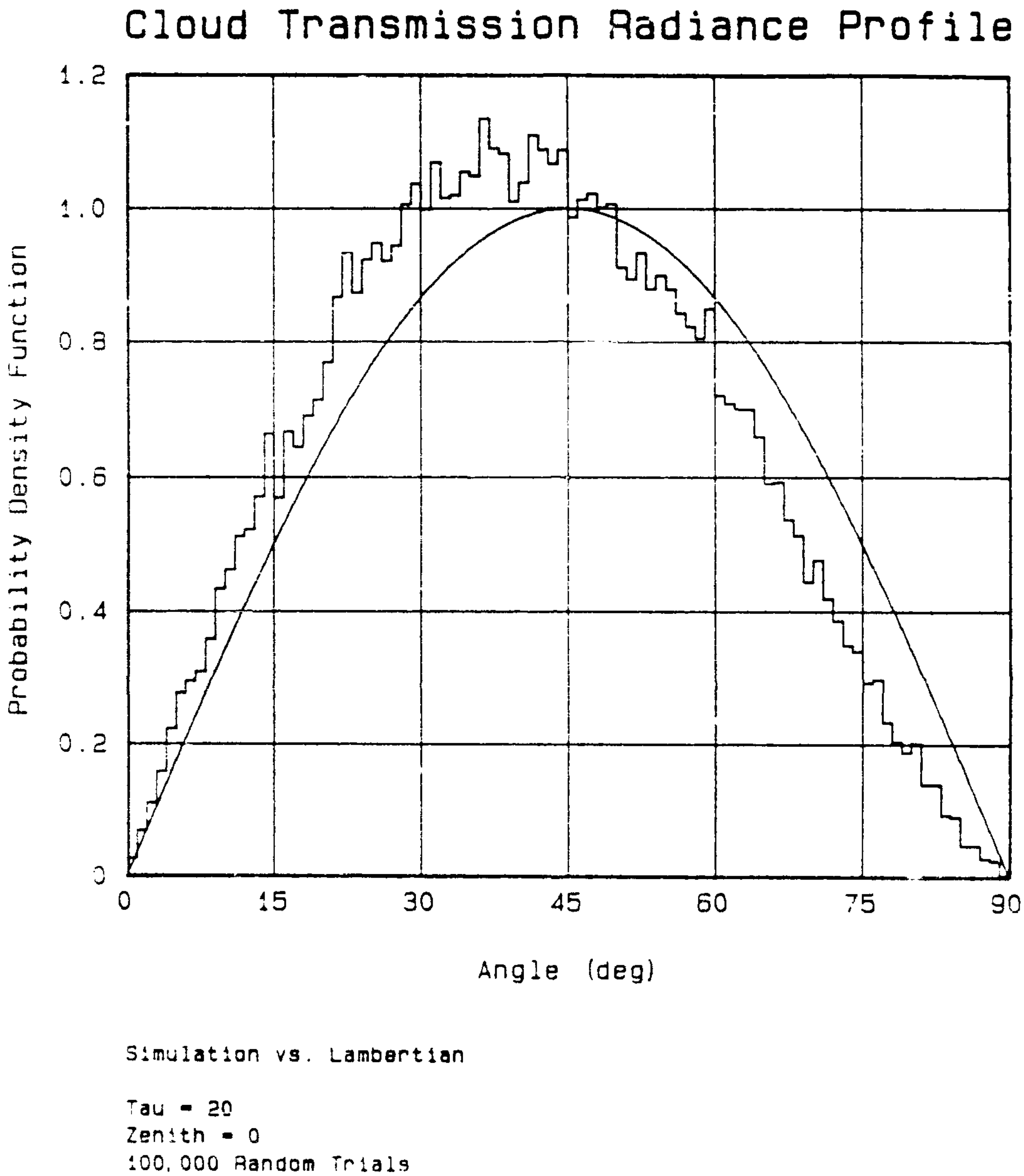

Figure 9. Comparison of Simulation and Lambertian Radiance Profile (Cloud Transmission)

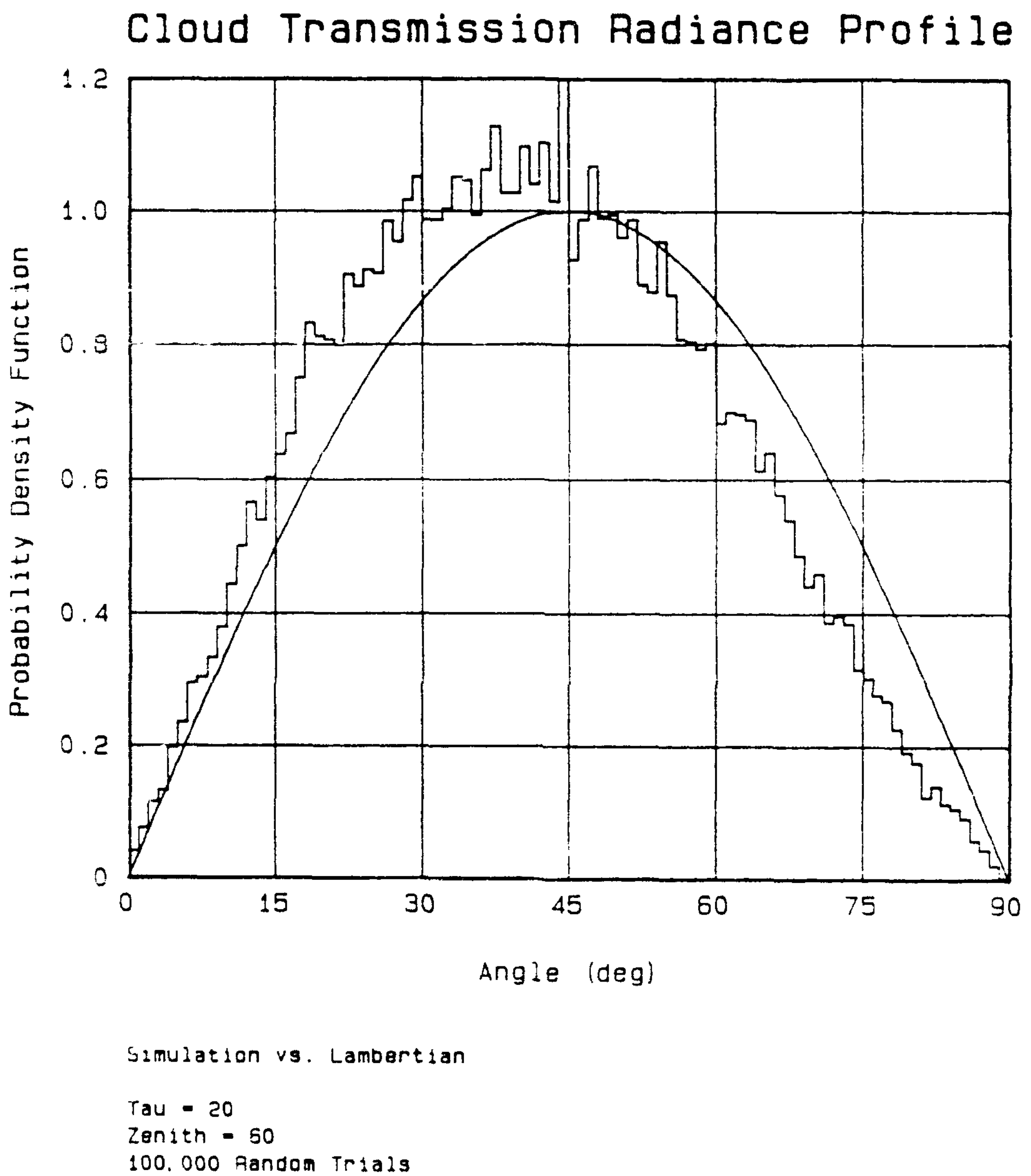

Figure 10. Comparison of Simulation and Lambertian Radiance Profile
(Cloud Transmission)

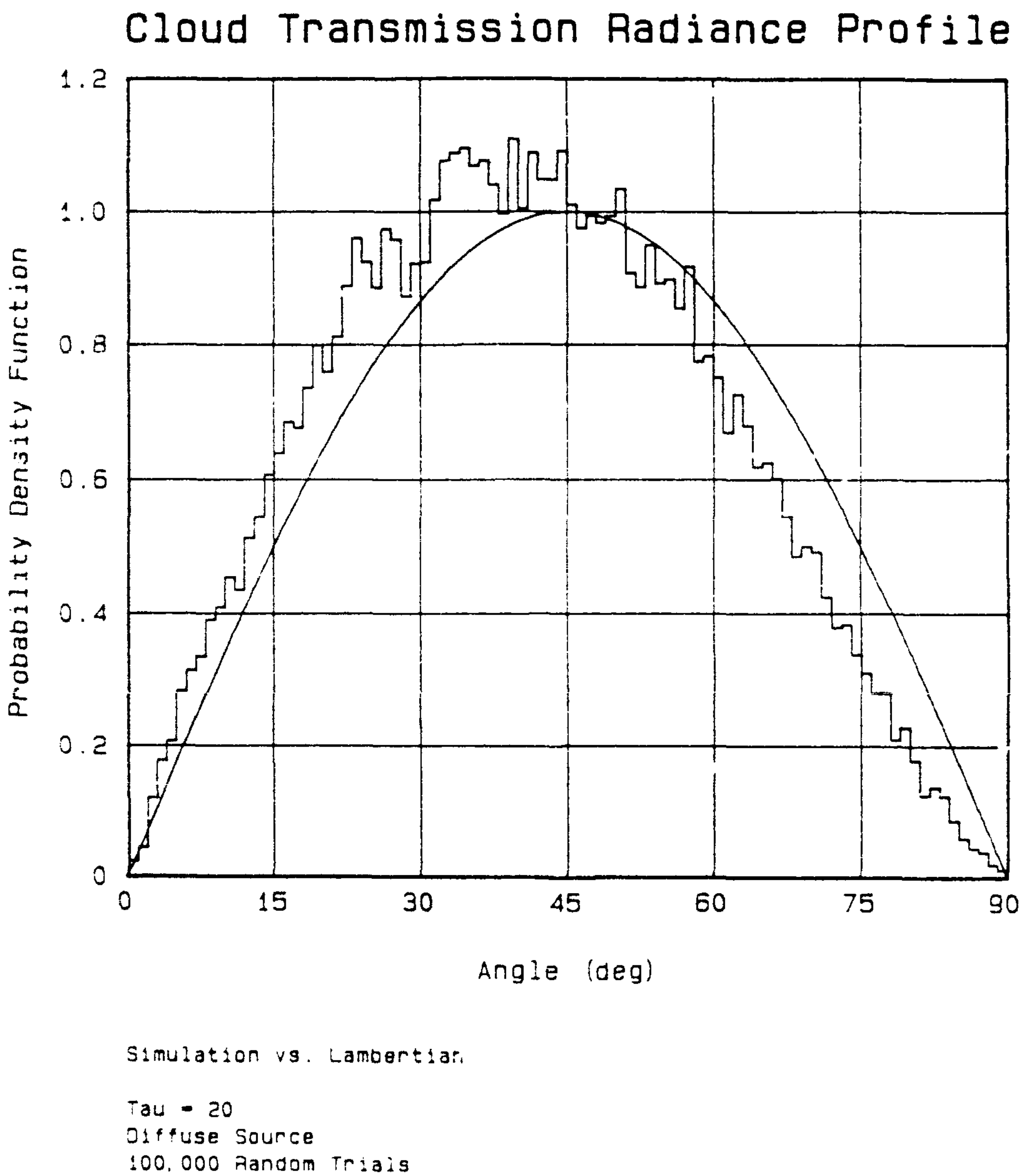

Figure 11. Comparison of Simulation and Lambertian Radiance Profile (Cloud Transmission)

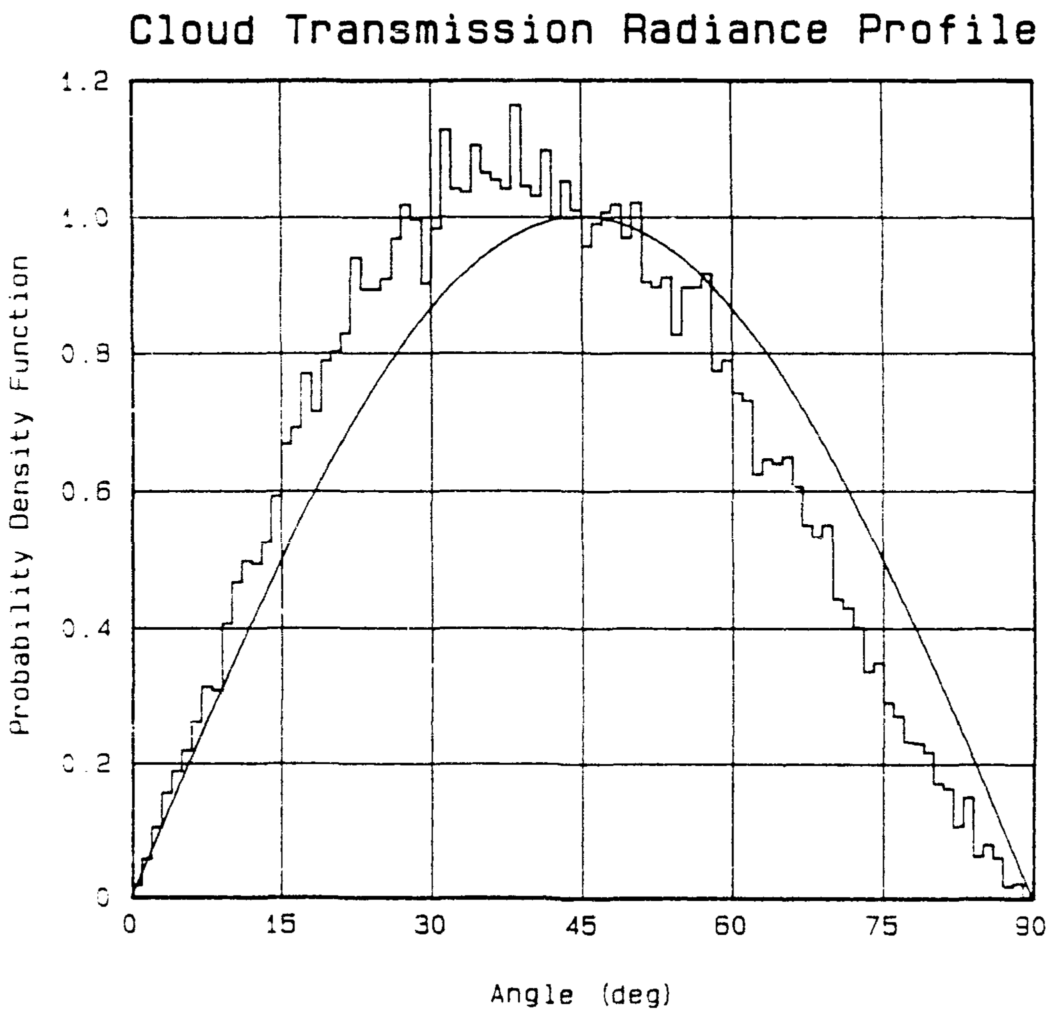

Simulation vs. Lambertian

Tau = 100
Zenith = 0
250,000 Random Trials

Figure 12. Comparison of Simulation and Lambertian Radiance Profile (Cloud Transmission)

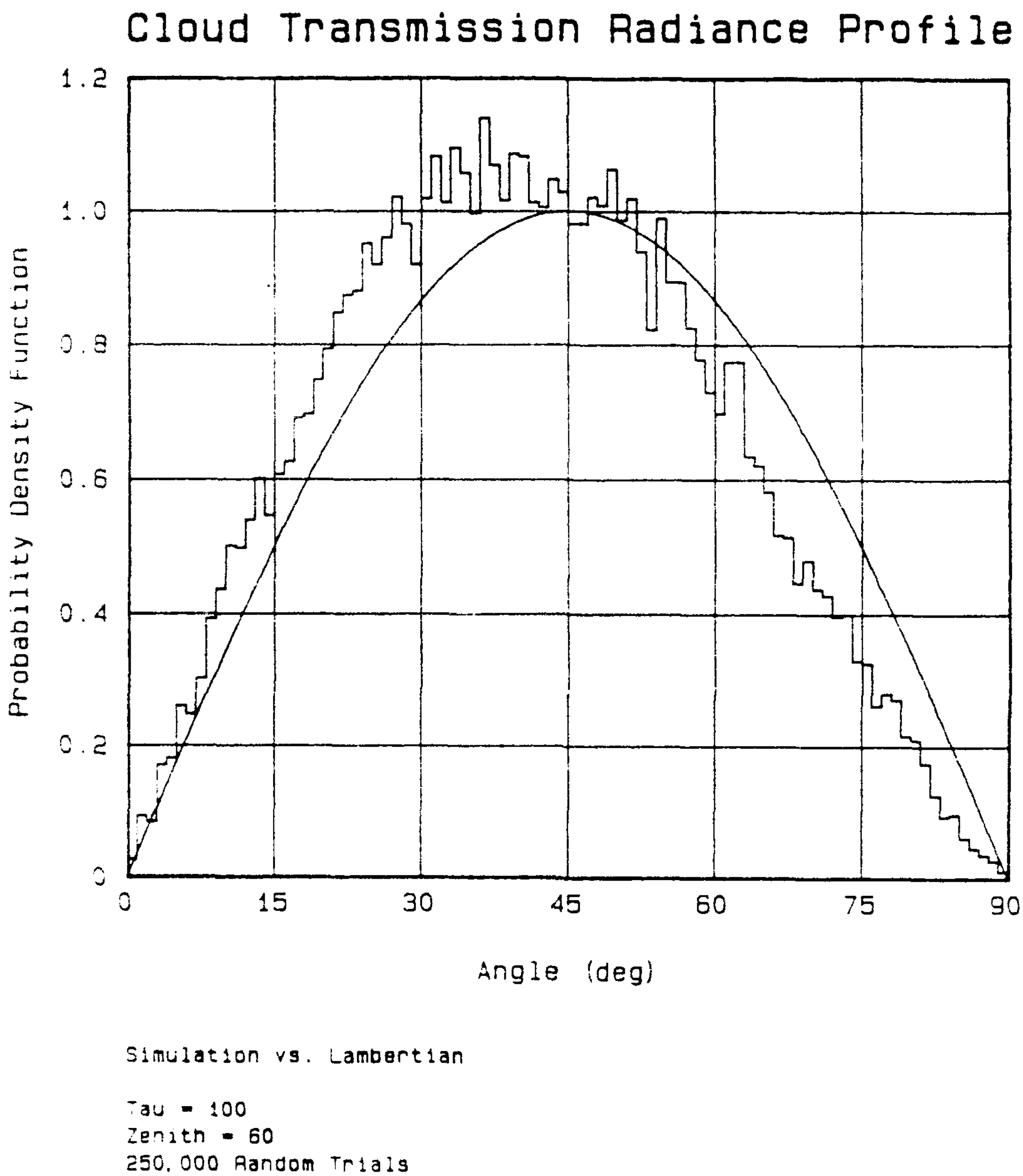

Figure 13. Comparison of Simulation and Lambertian Radiance Profile
(Cloud Transmission)

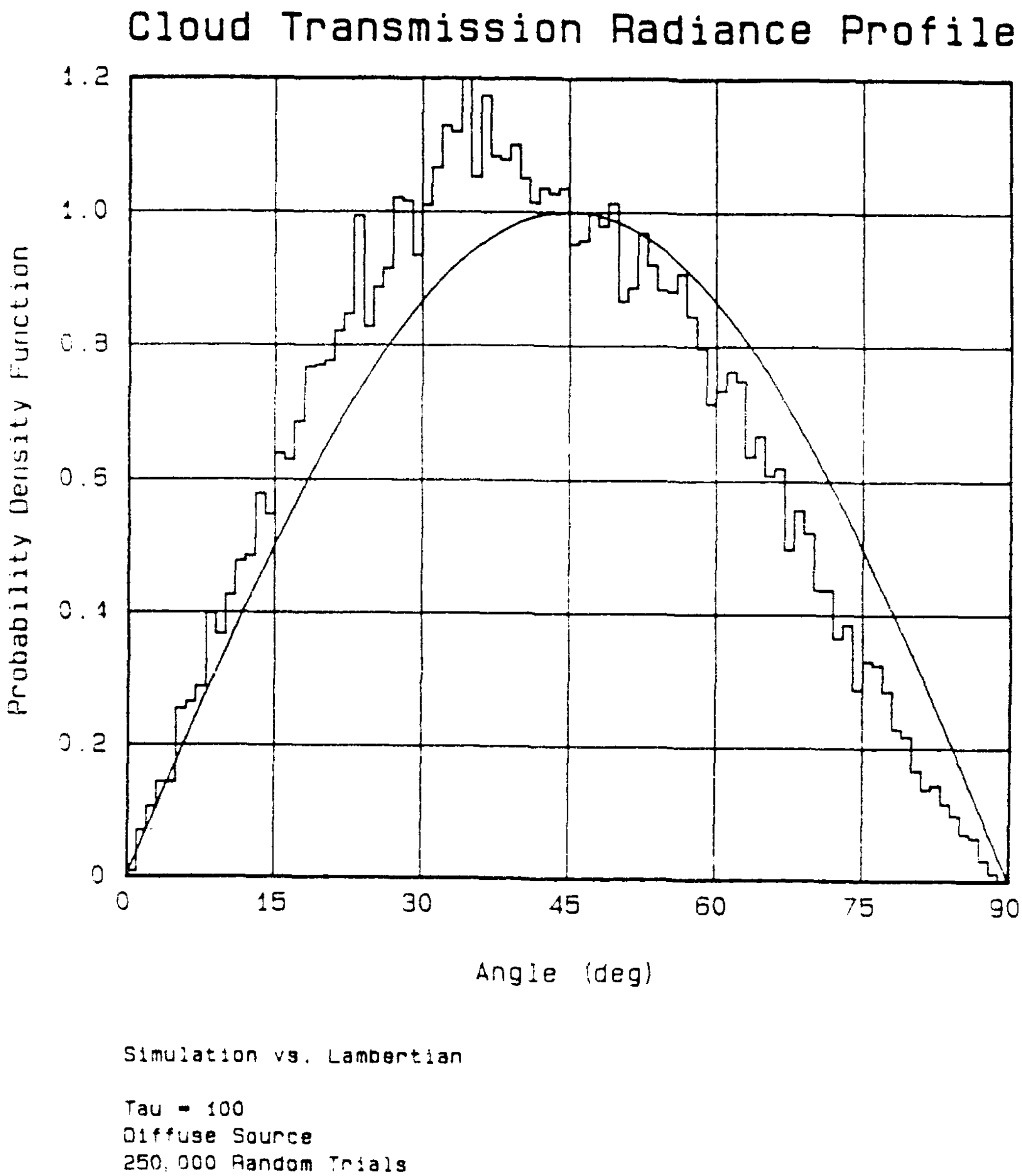

Figure 14. Comparison of Simulation and Lambertian Radiance Profile (Cloud Transmission)

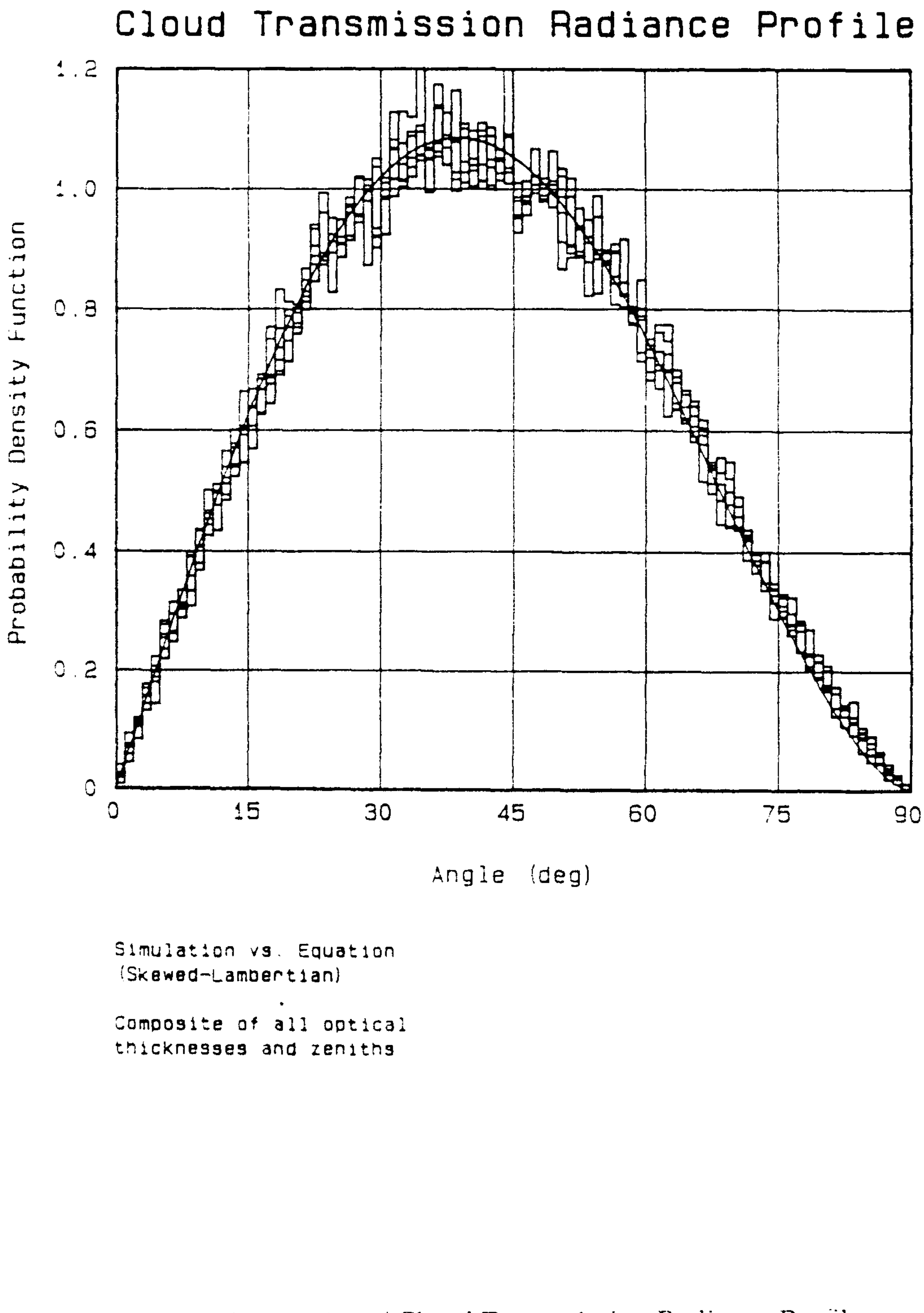

Figure 15. Composite of Cloud Transmission Radiance Profiles

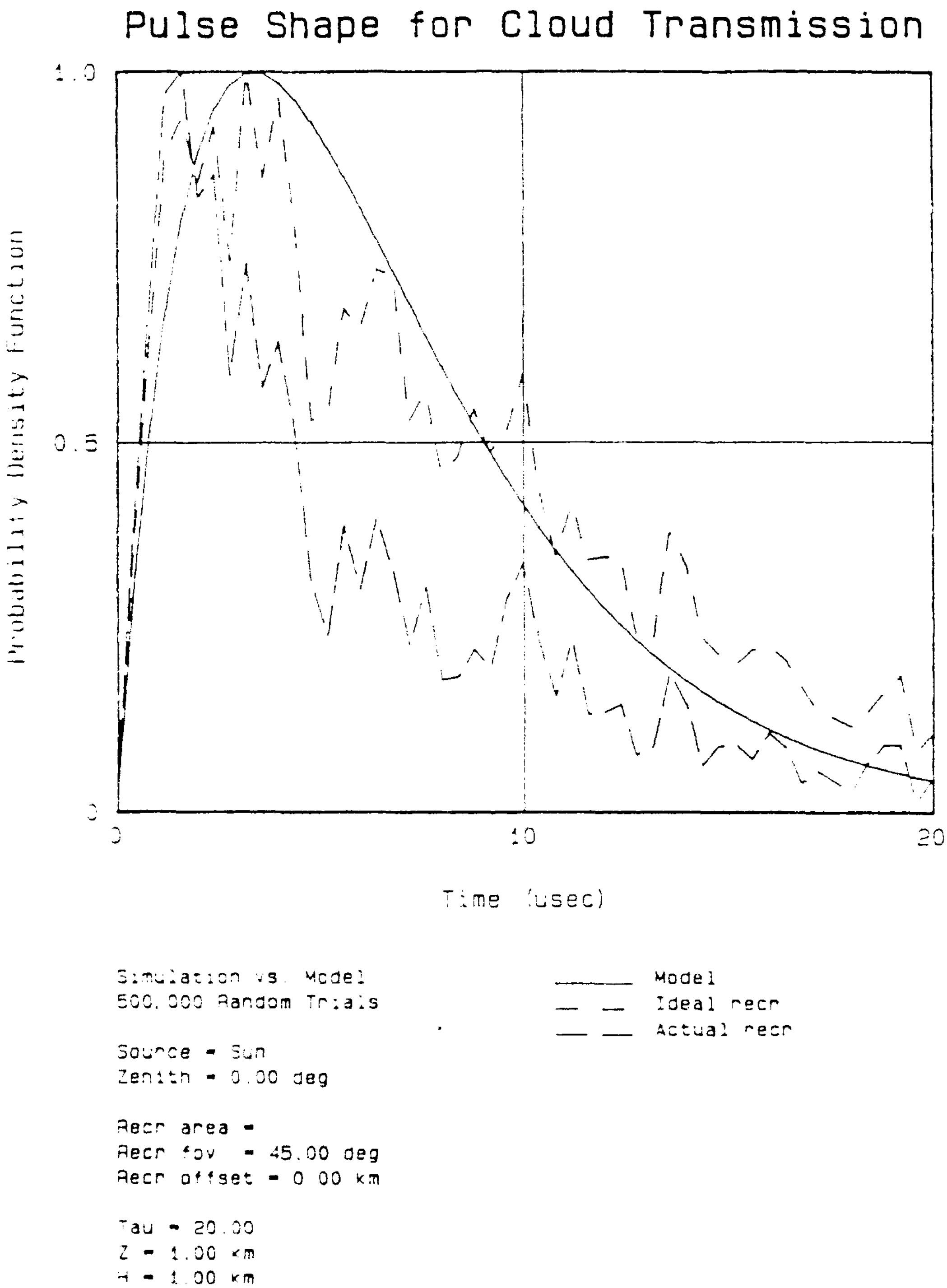

Figure 16. Comparison of Simulation and Model Pulse

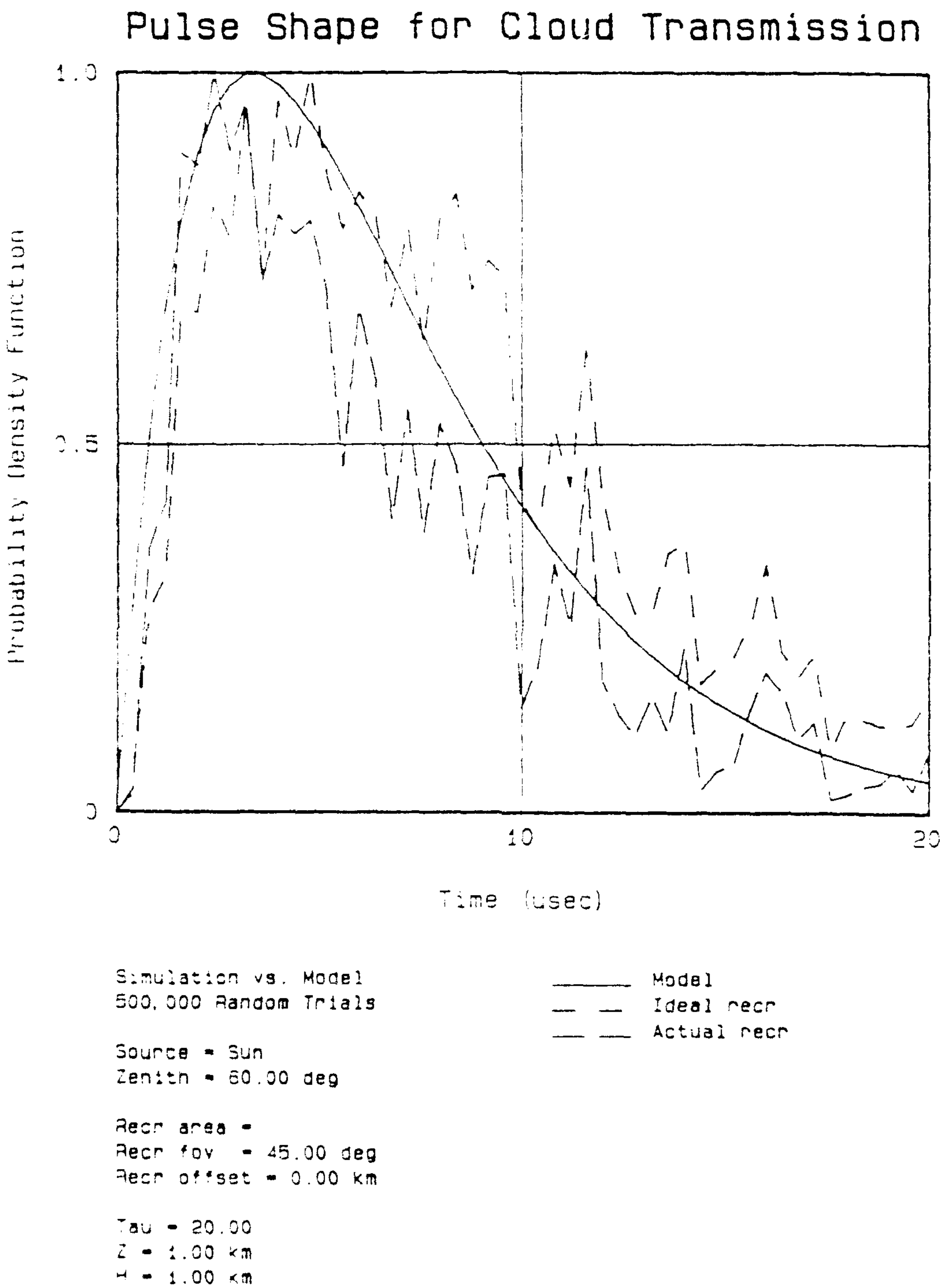

Figure 17. Comparison of Simulation and Model Pulse

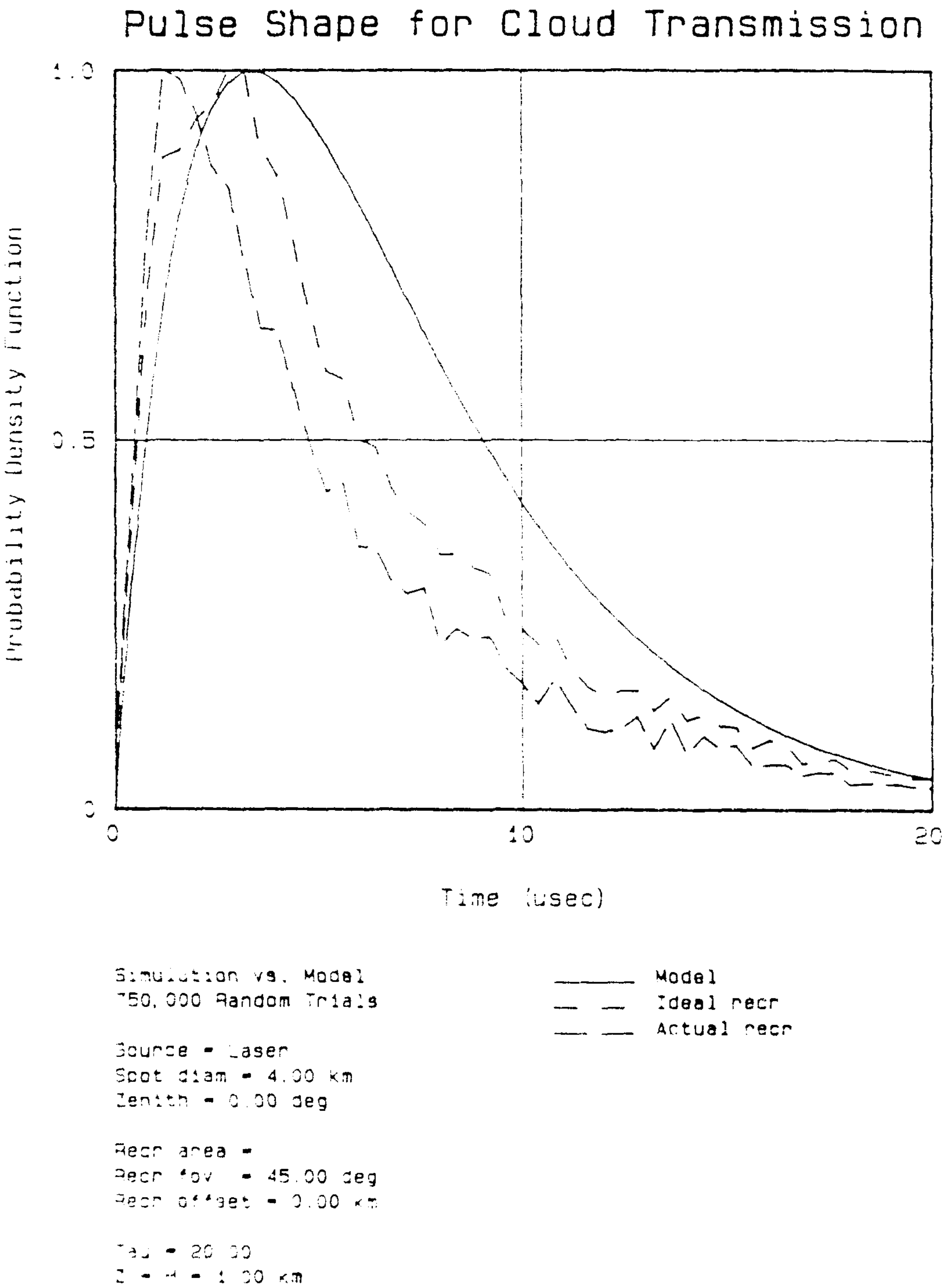

Figure 18. Comparison of Simulation and Model Pulse

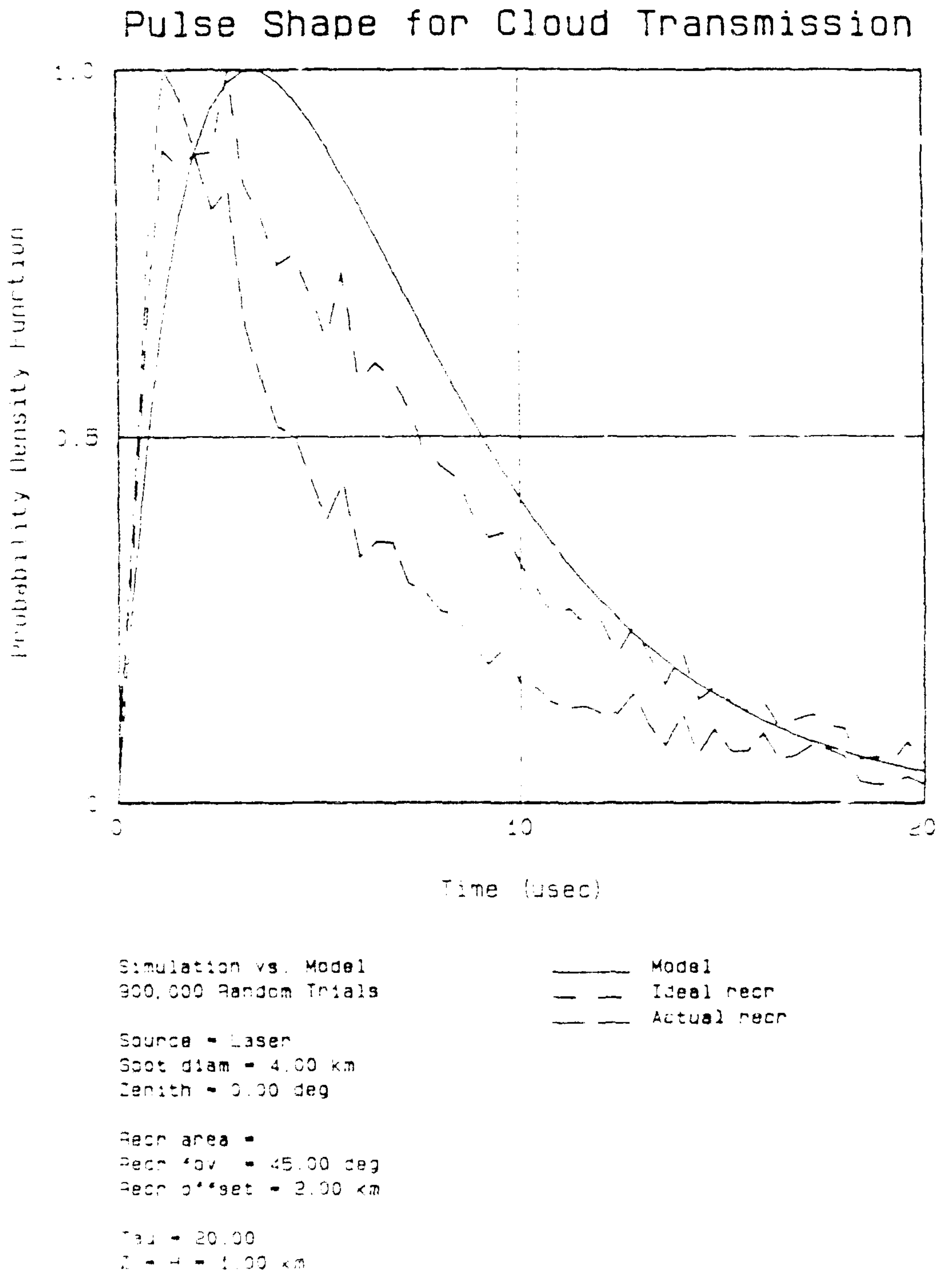

Figure 19. Comparison of Simulation and Model Pulse

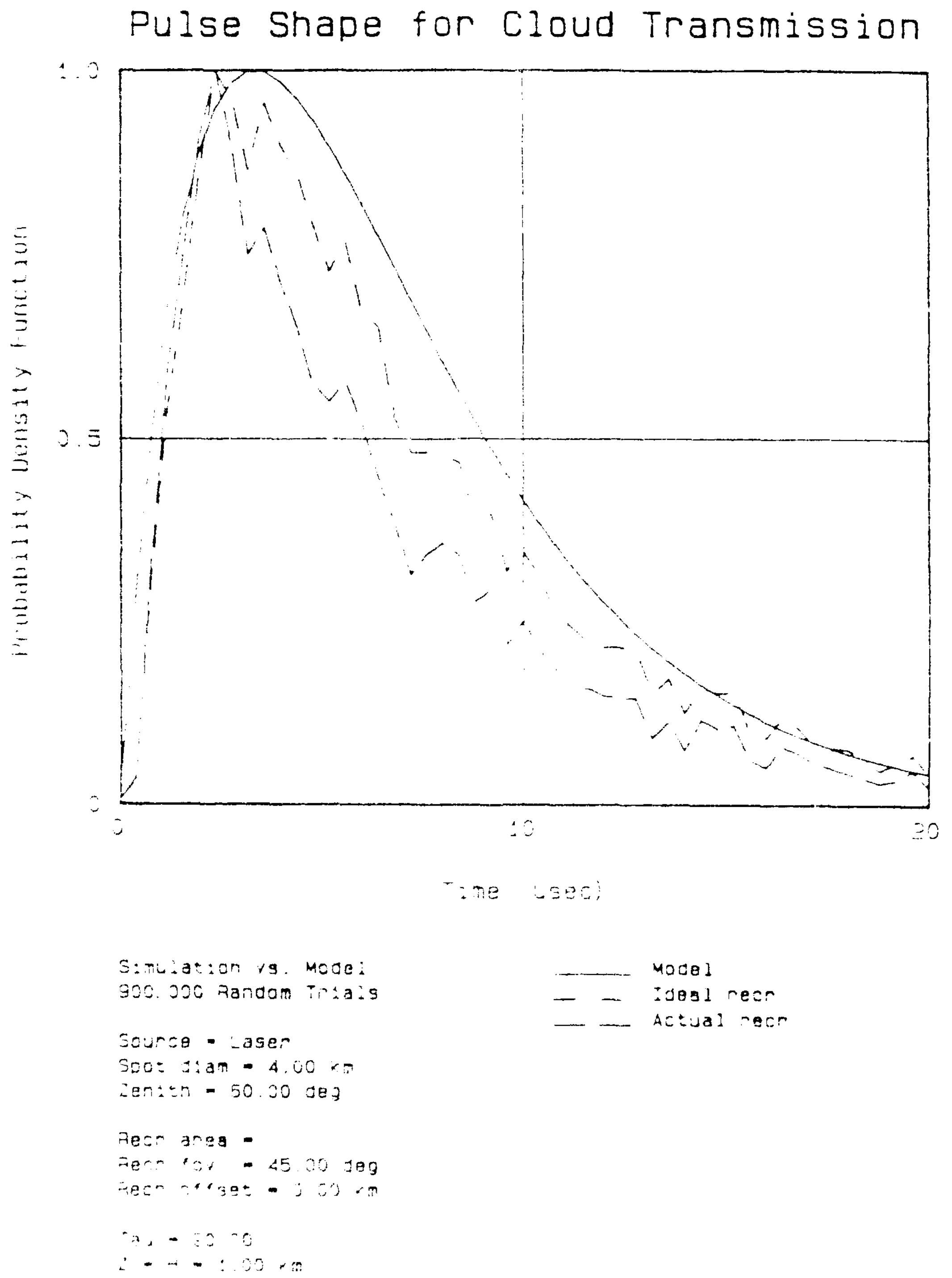

Figure 20. Comparison of Simulation and Model Pulse

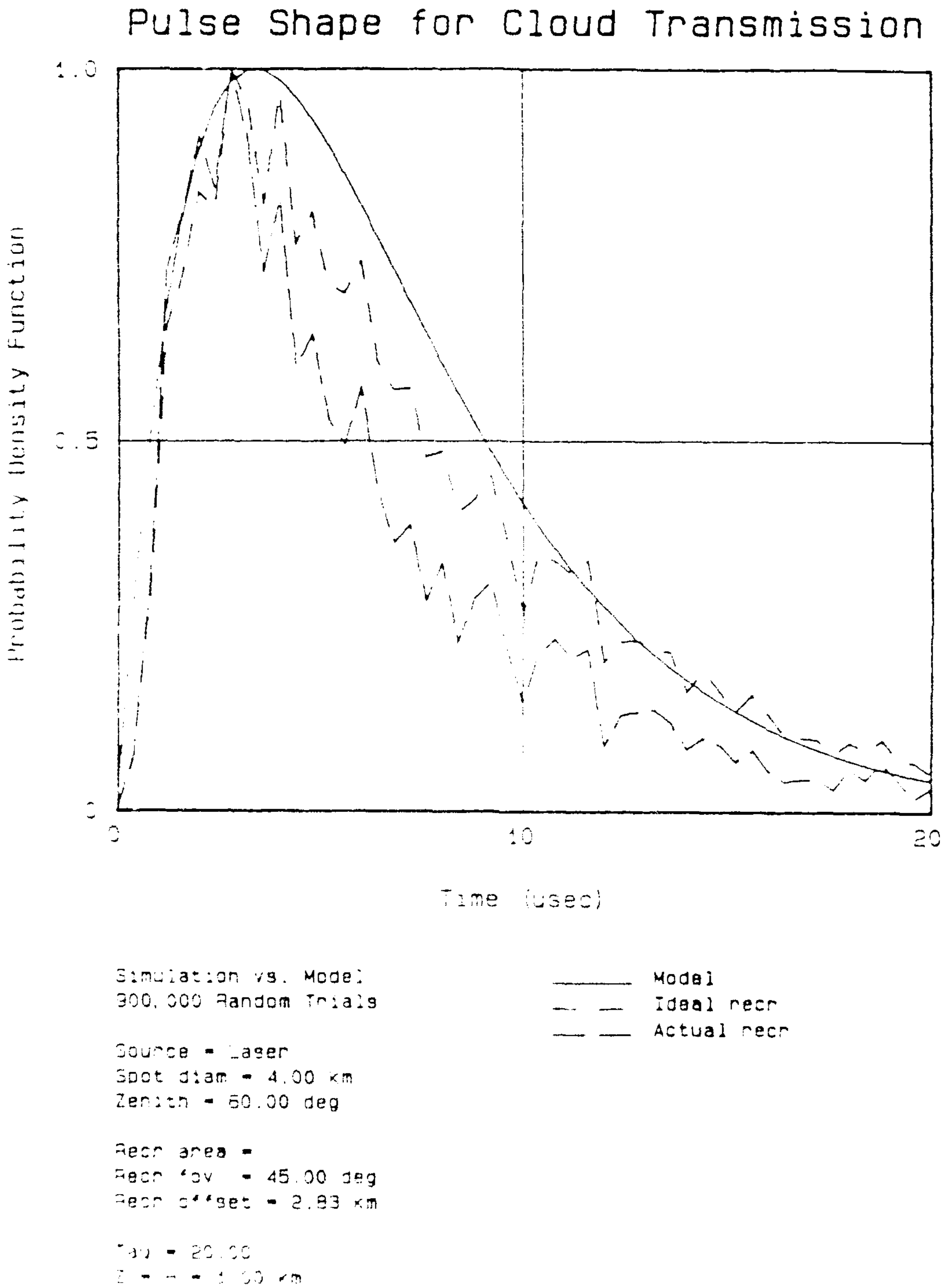

Figure 21. Comparison of Simulation and Model Pulse

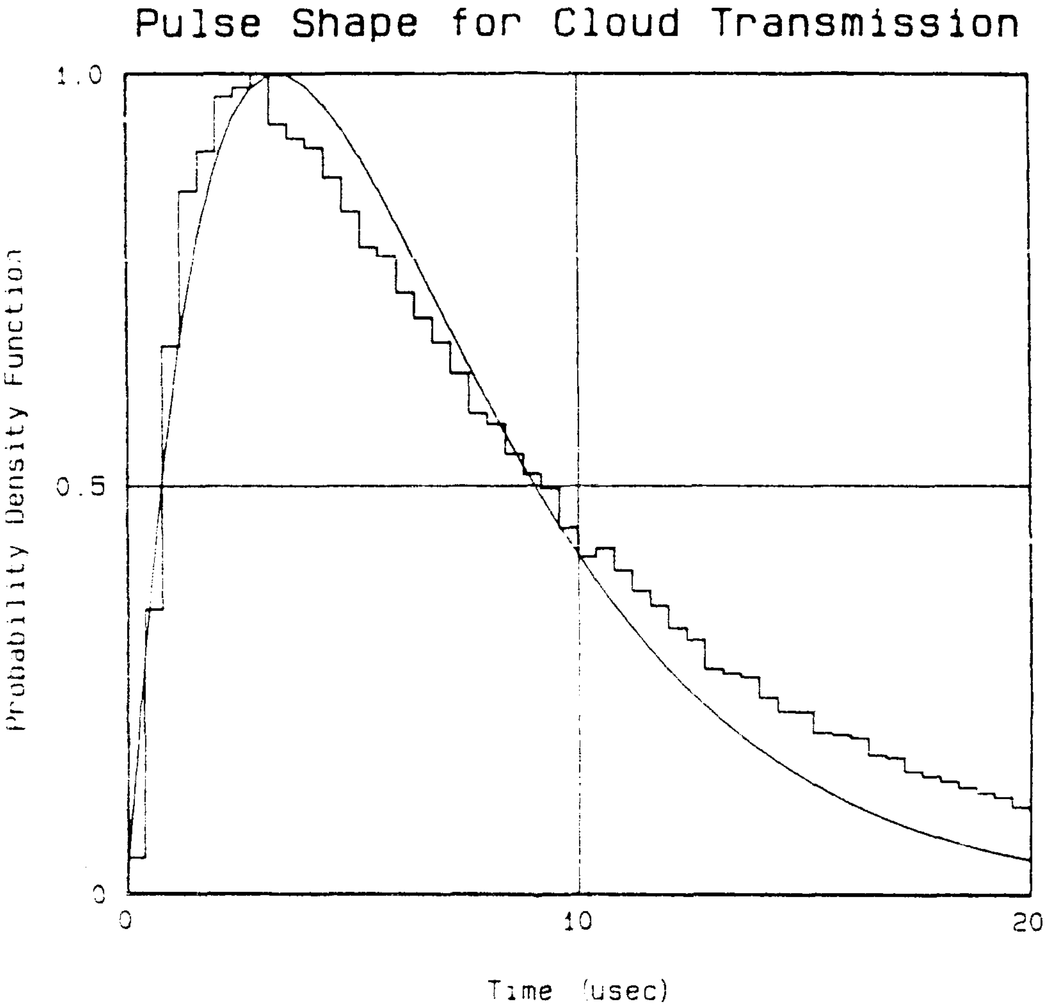

Simulation vs. Model
300,000 Random Trials

Point Source
Distrubuted Receiver
Zenith = 0.00 deg

Tau = 20.00
g = 0.850
Z = 1.00 km
H = 1.00 km

Figure 22. Comparison of Model with Simulation Pulse
(Point Source and Distributed Receiver)

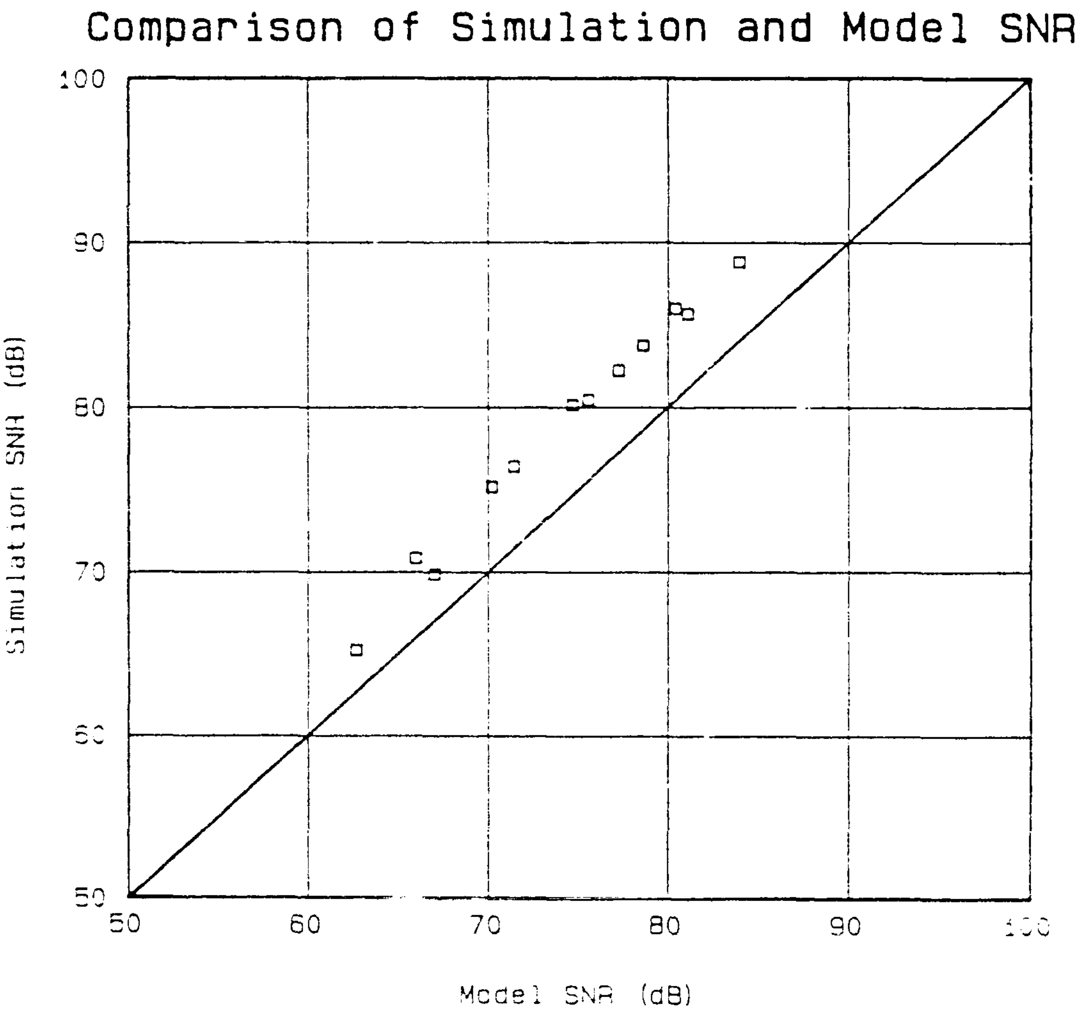

Sun zenith = 0/60 deg
Laser zenith = 0/60 deg
Laser spot = 2/5.64 km

Recr area =
Recr fov = 45.00 deg
Recr offset = variable
Spot extension matches
receiver offset

Tau = 20 (nominal)
Z = 1.00 km
H = 1.00 km

Figure 23. Comparison of Simulation with Model S/N Ratio

APPENDIX A. MONTE CARLO SIMULATION OF RADIATIVE TRANSFER

1.0 INTRODUCTION

The purpose of this Appendix is to give a brief introduction to and description of Monte Carlo simulation methods for radiative transfer problems. The Appendix is intended as an adjunct to the Monte Carlo codes developed for the Naval Ocean Systems Center; its function is to define the underlying basis of the codes and does not purport to be a primer on Monte Carlo simulations. The reader is referred to Kalos and Whitlock (1986) for a general discussion of Monte Carlo methods and to Lenoble (1985) for a discussion of its application to radiative transfer.

In a Monte Carlo computation one photon at a time is followed along its three-dimensional path through a scattering medium. Its fate is determined by suitable probability distributions for mean free path, absorption, scattering angle, wall absorption and reflection, and so on. The photon is followed until it is absorbed, detected, or leaves the field of interest. A sufficient number of photons are followed until a picture of the system emerges.

The Monte Carlo method has some advantages over other computational methods for radiative transfer, namely

- any phase function can be used
- can include polarization (with a two times penalty in computation time)
- several detectors may be included (small penalty in computation time)
- can divide medium into both vertical and horizontal layers of different optical properties (small penalty in computation time)
- complex geometries can be used (small penalty in computation time)

Naturally, there are disadvantages as well . . .

- not suitable if high accuracy is desired (doubling the accuracy requires quadrupling the computer time)
- always get bin averaged radiances rather than point values (smaller bins mean increased computation time for a given accuracy)
- not practical for optically thick media (say, $\tau > 100$)

A technical discussion of the Monte Carlo method for radiative transfer is presented in Section 2. The physics is described and the geometry of scattering is presented. Next, the statistical relationships required are reviewed. Then the probability

distributions for mean free path and scattering angles are discussed. Finally, some miscellaneous subjects such as absorption and reflection are discussed.

Section 3 contains a discussion of the computational aspects of Monte Carlo simulation. Program design philosophy and layout are discussed followed by a collection of tricks the author has found useful for reducing the computation time.

References and List of Figures are given in Sections 4 and 5, respectively.

2.0 TECHNICAL DISCUSSION

Figure A-1 shows a schematic of the scattering process. Photons are introduced into the scattering medium from a source with a specified mean free path and orientation. Upon encountering a scattering particle the photon is scattered off with a new mean free path and direction. When the photon is scattered, its departure direction is determined relative to its arrival direction. In order to properly follow the photon its position in absolute coordinates must be determined.

2.1 Geometrical Considerations

Figure A-2 shows a sketch of the geometry of scattering. The primed coordinate system is relative to the arrival direction (i.e., z' aligns with the direction of the arriving photon). The unprimed coordinate system is aligned with the absolute coordinates.

Consider a scattering event with a unit mean free path scattered at a zenith angle, θ' and azimuth angle, α' relative to the arrival direction. Then the following transformation of coordinates applies

$$\begin{aligned} x' &= \sin\overset{\theta'}{\alpha'}\cos\overset{\alpha'}{\theta'} \\ y' &= \sin\alpha'\sin\theta' \\ z' &= \cos\theta' \end{aligned} \quad \text{(A-1)}$$

$$\begin{aligned} x &= -y'\sin\alpha' + x''\cos\alpha' \\ y &= x''\sin\alpha' + y'\cos\theta' \\ z &= -x'\sin\theta' + z'\cos\theta' \end{aligned} \quad \text{(A-2)}$$

where

$$x'' = x'\cos\theta' + z'\sin\theta' \quad \text{(A-3)}$$

and

$$\theta^* = \cos^{-1} z$$
$$\alpha^* = \tan^{-1}\left(\frac{y}{x}\right) \qquad \text{(A-4)}$$

Equations (A-1) through (A-4) must be computed for each scattering event. This can literally be in the tens of millions for a modest simulation. Unfortunately, computation times can be quite large because of the trigonometric functions. After much experimentation with alternative computation schemes (including fast look-up tables) it was found that the entire calculation could be done much faster in terms of direction cosines, and that very few trigonometric calculations are required at all. In fact, as will be seen later on, even the scattering angle zenith can be randomly drawn in terms of its direction cosine. (The azimuth is still drawn as an angle, however.)

Referring to Figure A-3, the direction cosines of the translation vector $\overline{lx}$ from the point of scattering, $\bar{x}_1$ to the next collision $\bar{x}_2$ are given by

$$l_1 = \frac{l_1'' c - l_2'' l_2'}{\sqrt{1 - l_3''^2}} \qquad \text{(A-5)}$$

$$l_2 = \frac{l_2'' c + l_1'' l_2'}{\sqrt{1 - l_3''^2}} \qquad \text{(A-6)}$$

$$l_3 = -\sqrt{1 - l_3''^2}\, l_1' + l_3'' l_3' \qquad \text{(A-7)}$$

where

$$c = l_3'' l_1' + \sqrt{1 - l_3''^2}\, l_3' \qquad \text{(A-8)}$$

and l_i are the direction cosines of the scattered photon in absolute coordinates, l_i' are those in coordinates relative to the arriving photon, and l_i'' are those of the arriving photon in absolute coordinates. Notice that there is no explicit dependence on any angles.

For a mean free path of length d the final position $\bar{x}_2$ is determined from

$$\bar{x}_2 = \bar{x}_1 + d\,\bar{l} \qquad \text{(A-9)}$$

It has been shown that the photon position can be tracked by calculating its position from its previous position and translation vector. The translation vector is obtained from a randomly drawn mean free path, direction cosine of zenith, and azimuth angle.

2.2 Statistical Considerations

Referring to Figure A-4, $p(x)$ is called a probability density function and its integral $f(x)$ is called a probability distribution function. The definition of the probability density function requires that

$$p(x) \geq 0$$
$$\int_0^\infty p(x)dx = 1 \qquad \text{(A-10)}$$

The probability distribution function is a cumulative probability, i.e.,

$$P(X \leq x) = f(x) = \int_0^x p(t)dt \qquad \text{(A-11)}$$

The distribution function satisfies these three conditions:

1. $\lim_{x \to 0} f(x) = 0; \quad \lim_{x \to \infty} f(x) = 1$
2. $f(x) \geq 0; \quad f(y) \geq f(x)$ if $y > x$
3. $f(x)$ is continuous

Finally, to get a random variable x with a distribution function $f(x)$, choose a random number, RN, uniform in [0,1] and get x from the inverse function, i.e.,

$$x = f^{-1}(\mathrm{RN}) \qquad \text{(A-12)}$$

It is always worthwhile to test that an algorithm indeed samples $f(x)$. Several methods to check an algorithm can be used. The simplest consists of generating random variables and sorting the results of Eq. (A-12) into bins within the range of the random variable. This can then be compared with the probability density function. Several examples will be seen later on in connection with distribution functions of interest in radiative transfer.

2.3 Mean Free Path

Simulation of the distance traveled between collisions is calculated directly since the fraction of radiation transmitted through a given distance is also the probability of a photon traveling the same distance. Thus,

$$p(x) = \exp(-\tau) = \exp\left(-\int_0^s \beta\, ds\right) \tag{A-13}$$

$$f(x) = 1 - \exp(-\tau) \tag{A-14}$$

$$\int_0^s \beta ds = \tau = -\ln(1 - \mathrm{RN}) \tag{A-15}$$

If the scattering coefficient is constant then the mean free path is given simply by

$$s = -\frac{1}{\beta}\ln(\mathrm{RN}) \tag{A-16}$$

Figure A-5 shows a comparison of the statistical model, Eq. (A-16) with the probability density function. Eq. (A-13) (for a constant scattering coefficient). This demonstrates that applying Eq. (A-16) to random numbers uniform in [0,1] does indeed replicate the expected probability density function.

More generally, Eq. (A-15) must be iterated to get the mean free path, s. For a simple two-layer model, however, analytic results can also be obtained. The important point there is to adjust the mean free path if the photon goes from a region of one optical density to the other. Figure A-6 shows a sketch of the two-layer model.

Equation (A-15) suggests that a medium of continuously variable optical properties might be treated simply by transforming from the physical plane to that of the optical thickness, τ. This has never been tried by the author.

2.4 Scattering Functions

Many different scattering functions have been used in Monte Carlo simulations of radiative transport for different physical problems. Figure A-7 shows a sketch of the scattering geometry. The brief list below is limited to those with which the author is familiar:

- uniform distribution (usually applicable to the azimuth angle of scattering)
- isotropic (equal distribution of photons per unit solid angle; usually application to photon emission on quantum state transitions)
- Lambertian (equal distribution of photons per unit solid angle per unit area; usually applicable to reflection from surfaces)
- Mie scattering (complex scattering pattern caused by the interaction of electromagnetic waves with molecular dipoles characterized by strong forward scattering, usually applicable to scattering in aerosols and clouds). Figure A-8 shows a schematic of Mie scattering
- Henyey-Greenstein (an analytical model with characteristics of Mie scattering)
- Irvine-Henyey-Greenstein (an extension of the above model with improved backward scattering)
- Empirical (phase function and/or distribution are fit to experimental data; these have been used for clouds and sea water, for example)
- Skewed-Lambertian (cosine-to-the-*n* behavior)

Other possibilities abound as well. King and Harshvardhan (1986) and others have used phase functions derived from Mie scattering calculations for a cloud with a particle size distribution. Waldman (1988) has used curve fits to experimental data of Petzold (1972) to get the scattering function in sea water. Some specific examples are considered in detail below.

A. Uniform Distribution

An example of uniform distribution is the azimuth angle upon scattering. The angle is selected randomly from

$$\theta = 2\pi \, RN$$

where RN is uniform in [0,1].

B. Isotropic Distribution

Isotropic distribution applies, for example, to spontaneous emission of a photon during a change in quantum state such as fluorescence. Statistically, the intensity, or number of photons per steradian is constant, therefore

$$
\begin{aligned}
p_I(\theta) &= \sin\theta \\
f_I(\theta) &= 1 - \cos\theta \\
\mu &= \mathrm{RN}
\end{aligned}
\tag{A-17}
$$

(Notice that RN is functionally equivalent to 1-RN since RN is uniform in [0,1].)

C. Lambertian Distribution

This is applicable to diffuse reflection from a surface. Statistically, the radiance or number of photons per unit area, per steradian is constant, therefore

$$
\begin{aligned}
p_L(\theta) &= 2\sin\theta\cos\theta \\
f_L(\theta) &= 1 - \cos^2\theta \\
\mu &= \sqrt{\mathrm{RN}}
\end{aligned}
\tag{A-18}
$$

Figure A-9 shows a comparison of the statistical model and the probability density function.

D. Henyey-Greenstein Distribution

This is a commonly used model for Mie scattering. Although it lacks the details of the Mie scattering it has the general characteristics and often proves to be an adequate model for cloud and aerosol studies. Its principal advantage is its analytic form, viz.,

$$
\begin{aligned}
p_{HG}(\theta) &= \frac{(1-g^2)\sin\theta}{2(1+g^2-2g\cos\theta)^{3/2}} \\
f_{HG}(\theta) &= \left(\frac{1-g^2}{2g}\right)\left(\frac{1}{1-g} - \frac{1}{\sqrt{1+g^2-2g\cos\theta}}\right) \\
\mu &= \frac{1+g^2-\left(\dfrac{1-g^2}{1+g-2g\,\mathrm{RN}}\right)^2}{2g}
\end{aligned}
\tag{A-19}
$$

Figure A-10 shows a comparison of the statistical model and the probability density function.

E. Irvine-Henyey-Greenstein Distribution

The principal shortcoming of the Henyey-Greenstein phase function is its weak backward scattering lobe. The Irvine model attempts to correct this by summing two Henyey-Greenstein phase functions with positive and negative asymmetries, respectively. Thus,

$$\begin{aligned} p_{IHG}(\theta) &= a\,p_{HG}(\theta;g_1) + (1-a)\,p_{HG}(\theta;g_2) \\ f_{IHG}(\theta) &= a f_{HG}(\theta;g_1) + (1-a) f_{HG}(\theta;g_2) \end{aligned} \tag{A-20}$$

where a is the fraction of forward scattered photons. Generally, $g_1 > 0$ and $g_2 < 0$. The direction cosine must be obtained from the distribution function by iteration. Figure A-11 shows a comparison of the statistical model and the probability density function.

F Sea Water Scattering Distribution

The Henyey-Greenstein phase function is not generally adequate to model scattering of light in sea water because a high absorption coefficient puts a stronger emphasis on the forward and backward scattering lobes. Statistical models for the sea water scattering distribution function can be developed from empirical data, such as that presented by Petzold (1972).

Figure A-12 shows a comparison of such a statistical model (curve fit to data) and the probability density function (data on the volume scattering function in sea water).

G. Skewed-Lambertian

There are no specific applications for this distribution. Frequently, however, one encounters radiance profiles which are described as having "cosine-to-the-n" behavior, i.e.,

$$\begin{aligned} p_{SL}(\theta) &= (n+1)\cos^{n}\theta\,\sin\theta \\ f_{SL}(\theta) &= 1 - \cos^{n+1}\theta \\ \mu &= RN^{\frac{1}{n+1}} \end{aligned} \tag{A-21}$$

Figure A-13 shows a comparison of the statistical model and the probability density function.

2.5 Surface Reflection

Surface reflections may be diffuse or specular. One special case of diffuse reflection is Lambertian, in which the reflected radiance is the same in all directions. Figure A-12 shows a sketch of the reflected irradiance for various types of surface reflection.

A commonly encountered problem in radiative transfer is the specular reflection of photons off curved surfaces. Here the vector form of Fermat's principle is required to determine the direction of the reflected photon,

$$\bar{r}'' = \bar{r} - 2(\hat{n} \cdot \bar{r})\hat{n} \tag{A-22}$$

where $\bar{r}$ and $\bar{r}''$ are the incident and reflected directions, respectively, and $\hat{n}$ is the unit normal to the surface (see Figure A-12).

When the walls have discontinuous first derivatives (i.e., corners, as in the boundary of a wall and floor) then special attention must be paid to the photon reflection. As unlikely as such an encounter may be in a simulation, experience has shown that it can and will happen, often with dire consequences in a program which did not anticipate it.

2.6 Absorption

Absorption can occur within the scattering medium or at a surface. In either case the probability of the photon being absorbed can be computed and the photon path can be continued, or not, depending on the outcome.

This can be very inefficient from a computational point of view, however. Rather, what is recommended is that each photon is assigned a weight, or probability, which is diminished upon each absorption. The decrease in photon weight is just the probability that it was absorbed. In this way the computation can proceed without starting a new photon each time one is absorbed.

2.7 Gaussian Radiance Profile

This special topic is of relevance to photon detection under water where the radiance profile is typically Gaussian (see, for example, Jerlov, 1976). There are many ways to generate random variables which replicate Gaussian probability density functions, but these density functions are not the same as those associated with a Gaussian *radiance profile*. The difference is that the radiance profile contains an additional cosine term (for the area effect) and a sine term (for the solid angle effect).

In a formal sense the probability density function for a Gaussian radiance profile for a specific receiver is given by

$$p(\theta) = \frac{\int_0^{\theta} \exp\left(-\left(\frac{\theta}{\sigma}\right)^2\right)\cos\theta \, \sin\theta \, d\theta}{\int_0^{\theta_{fov}} \exp\left(-\left(\frac{\theta}{\sigma}\right)^2\right)\cos\theta \, \sin\theta \, d\theta} \tag{A-23}$$

where θ_{fov} is the receiver field of view half-angle. It has been assumed that the receiver has a cosine response (otherwise substitute the response function for $\cos\theta$).

The probability of integrating this in closed form, then determining the distribution function and its inverse, is zero. Waldman (1987) has found a suitable approximation for the exponential term which permits integration of Eq. (22). Nevertheless, the distribution function is cumbersome and the direction cosine can only be obtained by iteration. This is somewhat time consuming and a table look-up is preferred. Figure A-13 shows a comparison of the statistical model and the probability density function for a receiver with a 90° field of view half-angle (flat plate receiver).

2.8 Monte Carlo Simulation Results

Several kinds of results can be gleaned from Monte Carlo simulations. These can be broadly characterized as global, statistical, and specific. As an example, consider light transmission from a point source through a cloud. Global results consist of the total number of photons reflected and transmitted. Statistical information might consist of the mean and rms values for exit radius, angle, and time. The mean and rms are calculated as follows:

$$\bar{y} = \frac{\sum_{i=1}^{N} y_i w_i}{\sum_{i=1}^{N} w_i} \tag{A-24}$$

$$\overline{y^2} = \frac{\sum_{i=1}^{N} y_i^2 w_i}{\sum_{i=1}^{N} w_i} \tag{A-25}$$

$$y_{rms} = \sqrt{\overline{y^2} - (\bar{y})^2} \qquad (A\text{-}26)$$

where y_i are the functions being evaluated (e.g., exit radius, angle, or time) and w_i is a weighting function. The weighting function applies in such cases where the photons may arrive at the exit plane with different weights (e.g., due to absorption). These statistics can be computing on a running basis so that it is not necessary to store all of the individual results (which would be impractical, if not impossible, on most computers).

Specific results refer to such information as the radiance profile, surface energy distribution, and pulse temporal distribution. The nature of the Monte Carlo simulation is that these cannot be determined exactly, but rather only as bin averaged quantities. To collect this information requires separating the results (e.g., exit angle) into discrete bins and accumulating the weighted photons that arrive in each bin. These data can then be plotted as histograms to give an approximate picture of the photon behavior. Clearly, this contains the most information of all the results but can be particularly time consuming, depending upon the bin resolution.

3.0 COMPUTATIONAL ASPECTS

Monte Carlo simulations only exist because of computers, there are no analytical solutions. Program design and layout will dictate how useful the program is in meeting a variety of needs. Program execution speed is vital in determining if the program is useful at all.

3.1 Program Design Philosophy and Layout

A properly designed Monte Carlo simulation program should be readily adaptable to any number of radiative transfer problems within a broad class of such problems. To some extent this means anticipating which parameters are fixed and which are variable. Also the program should be highly modularized so that any part can be readily identified and altered as needed. Self-documenting programs can be very easy to maintain and modify. This can be achieved by assigning appropriate variable names that are either descriptive or conform to the standard notation of the field. Also, identifying all the constants, parameters, and variables, and their units, along with a modest amount of comments in the code is indispensable.

Frequently, it is desirable to examine a simulation periodically to see if the detailed results are adequately represented. The ability to stop and re-start the program makes this possible. Also, the program code should be relatively portable in order to

take advantage of faster machines and compilers as they become available. During program development it is desirable to test modules independently and also to build in debugging statements which can be turned on at will . (Actually, with modern compilers and debuggers this is probably not necessary.) Finally, the programming should be kept simple. There are times when this will be in direct conflict with making the program as fast as possible. Of course, make the program run faster, but document the simple procedure and the origin of the more arcane one in the code itself.

3.2 Program Execution Speed

In Monte Carlo simulations program execution speed may mean the difference between getting an answer or not. Methods of increasing program speed fall into two categories, general and ad hoc. General methods consist of programming practices which are germane to all simulations. For example, it has already been mentioned that trigonometric calculations are slow compared to those for direction cosines. This applies to scattering statistics as well, where the direction cosines can be found directly. Along the same lines, $\sqrt{1-\mu^2}$ is much faster than sine function; just beware of angles between π and 2π. Frequently, look-up tables can be faster than computation and can contain enough entries so that interpolation is not required. Using pointers to the table (available in the Pascal and C languages) is even faster. Avoid loops, particularly for updating direction cosines in position. There is a large computational overhead involved with a loop. Finally, use the fastest floating point representation available on the target machine and compiler; there are no hard and fast rules on this. On some machines/compilers reals are faster than doubles because the data fetches are quicker, while on others, they are slower because the numerical coprocessor must convert all the reals to doubles anyway! Of course, these considerations may be overridden by questions of numerical precision and range.

When dealing with specific problems some ad hoc tricks may be found that can reduce computation time significantly. Without any elaboration, these may consist of selective generation of photons (i.e., ignoring ones which initially go off in the wrong direction), discarding photons which stray too far, calculating several cases at once if possible (e.g., several receiver locations, different wavelength photons, etc.), simplify complex media (e.g., in an atmospheric transmission problem treat a cloud as a diffuse reflector rather than simulating it), exaggerate receiver size to collect more photons, cheat on receiver shape to simplify detection calculation, and so on.

One method of speeding up the calculations computes the probability of a photon reaching a detector rather than just collecting those photons which actually do reach it. The model is invaluable and some cases and not applicable at all in others. It is called the intensity reference method and it is discussed separately in Appendix B.

4.0 REFERENCES

Jerlov, N.G. (1976). *Marine Optics,* Elsevier Scientific Publishing Company, Amsterdam.

Kalos, M.H. and Whitlock, P.A. (1986). Monte Carlo Methods, Volume 1: Basics, John Wiley & Sons, New York.

King, M.D. and Harshvardhan (1986). "Comparative Accuracy of the Albedo, Transmission, and Absorption for Selected Radiative Transfer Approximations," NASA Reference Publication 1160.

Lee, G., et al. (1985). "SLCAIR Report," Titan Systems, Inc.

Lenoble, J., editor (1985). *Radiative Transfer in Scattering and Absorbing Atmospheres: Standard Computational Procedures,* A. Deepak Publishing, Hampton, Virginia.

Petzold, T.J. (1972). "Volume Scattering Functions For Selected Ocean Waters," Scripps Institution of Oceanography, Visibility Laboratory, SIO Ref. 72-78.

Waldman, C.H. (1987). "Receiver Field of View Function," report prepared for Titan Systems, Inc.

Waldman, C.H. (1988). Private communication.

5.0 LIST OF FIGURES

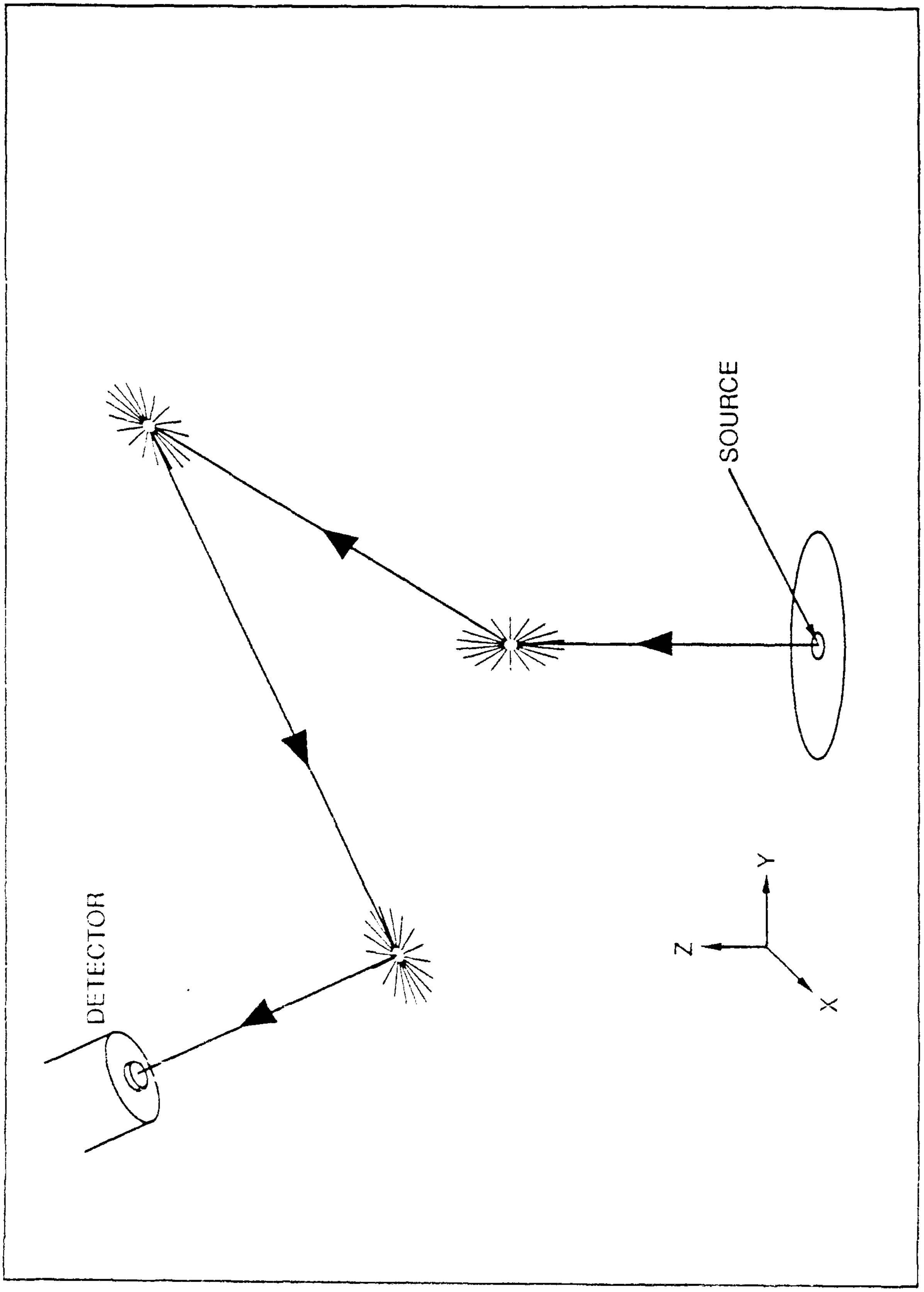

Figure A-1. Schematic Drawing—Physical Description

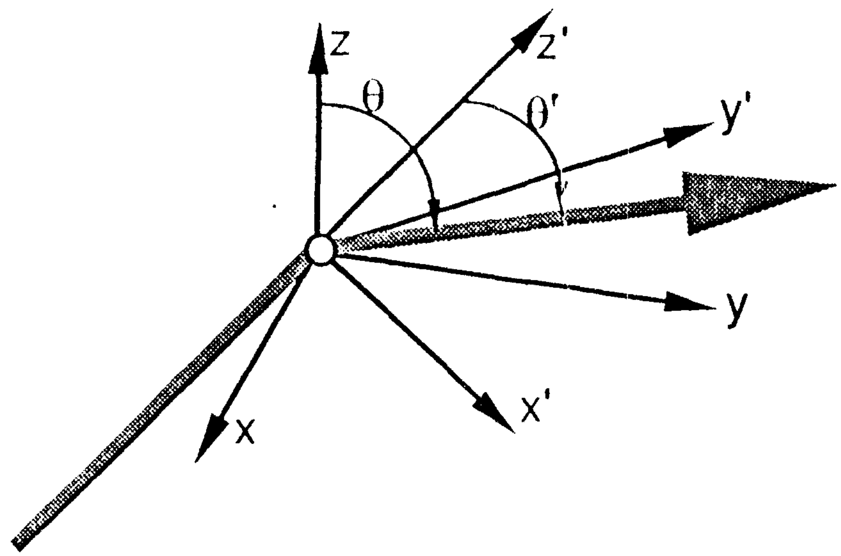

$$x' = \cos\theta' \sin\alpha'$$
$$y' = \sin\alpha' \sin\theta'$$
$$z' = \cos\theta'$$

$$x = \cos\alpha' x'' - \sin\alpha' y'$$
$$y = \sin\alpha' x'' + \cos\alpha' y'$$
$$z = -\sin\theta' x' + \cos\theta' z'$$
$$x'' = \cos\theta' x' + \sin\theta' z'$$

$$\theta' = \cos^{-1} z$$
$$\alpha = \tan^{-1} \frac{y}{x}$$

Note:
Each new scattering is computed relative to the photon's direction of travel and must be transformed to the reference coordinate system.

Figure A-2. Geometrical Considerations

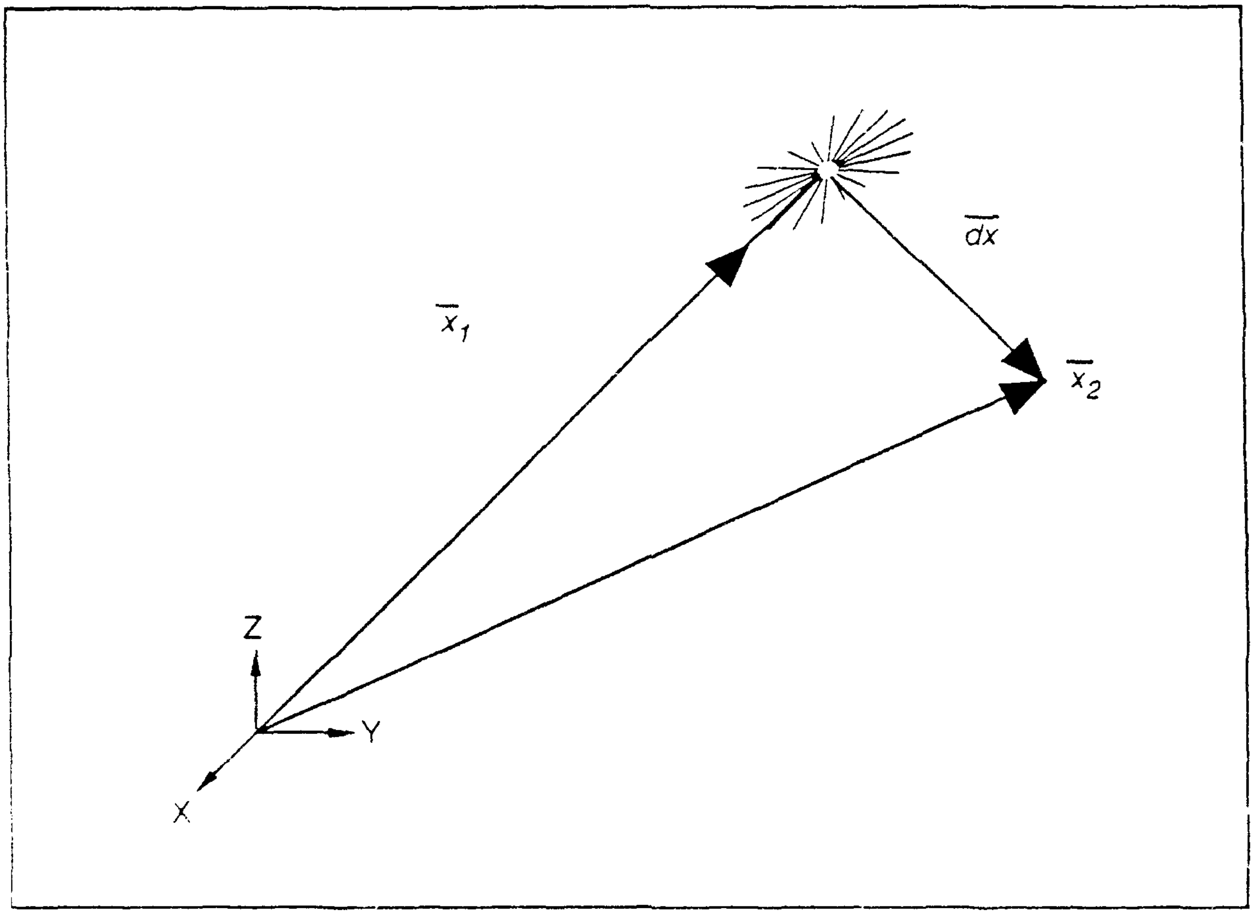

Figure A-3. Schematic of Single Scattering Geometry

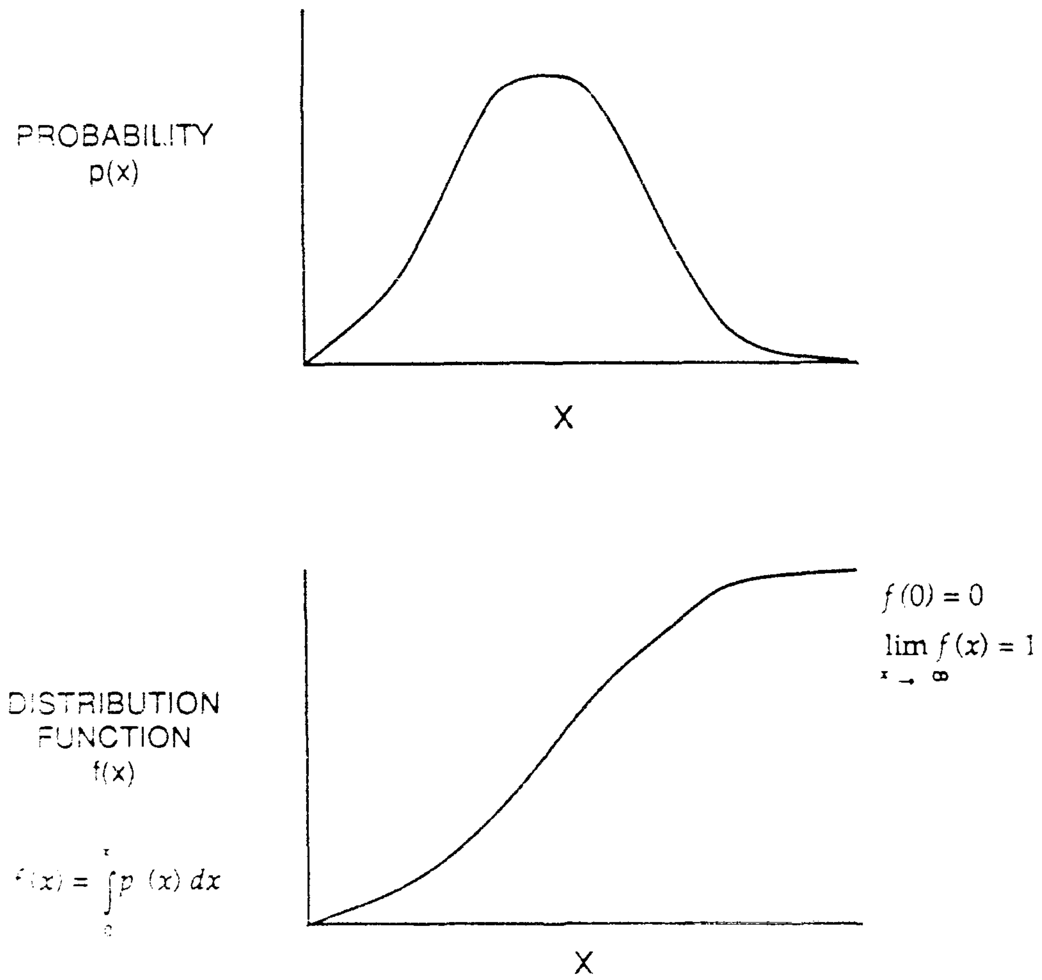

To get a random variable x with the distribution function f(x), choose a random variable, RN, uniform in [0, 1] and get x from the inverse function, i.e.,

$$x = f^{-1}(RN)$$

Figure 4. Statistics for Distribution

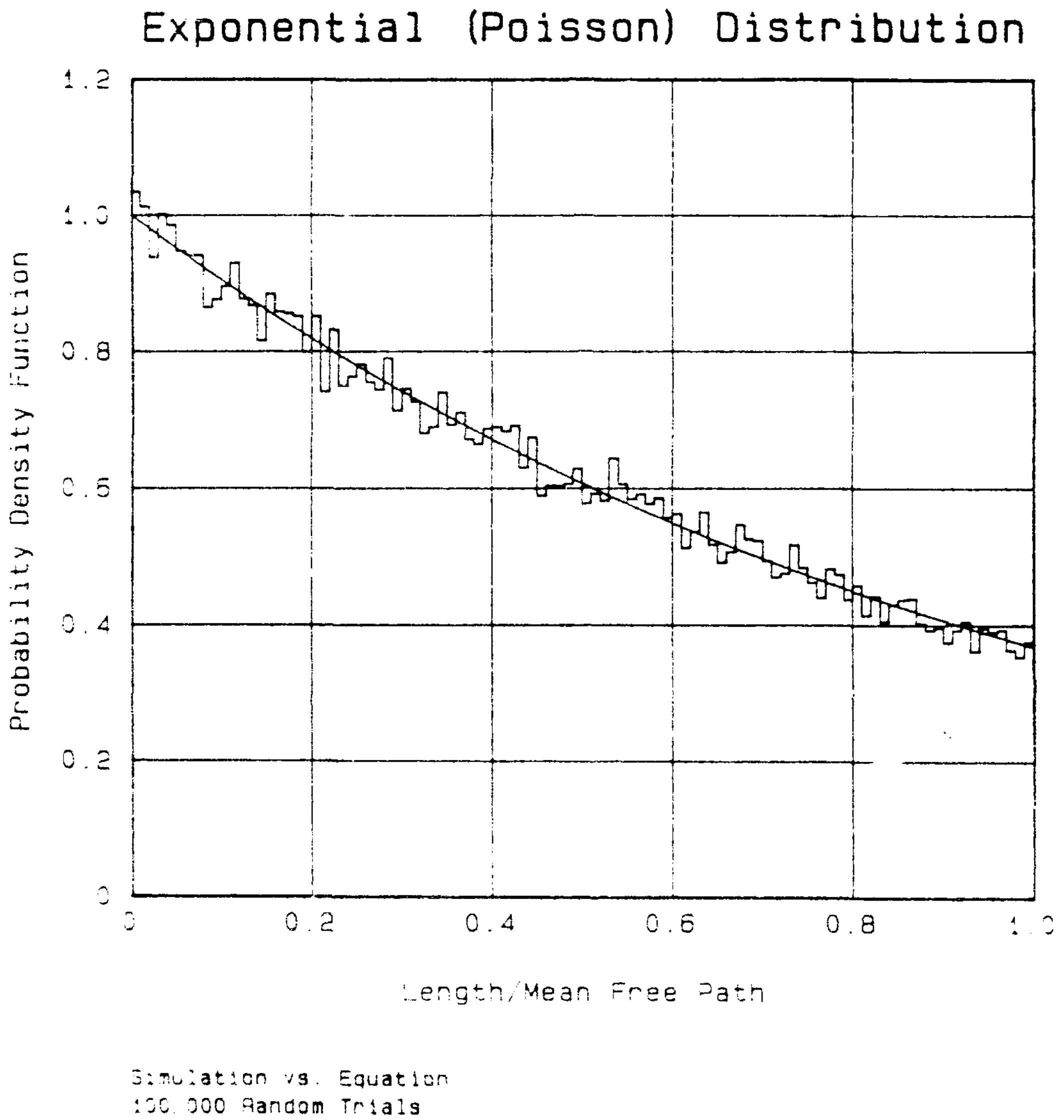

Figure A-5. Comparison of Simulation and Equation: Exponential (Poisson) Distribution

Simulation of the distance traveled between collisions is calculated directly since the fraction of radiation transmitted through a given distance is also the probability of a photon traveling the same distance.

$$p(x) = e^{-\tau} = e^{-\int_0^s \beta ds}$$

$$f(x) = 1 - e^{-\tau}$$

$$\int_0^s \beta ds = \tau = -\ln(1 - RN)$$

In general, s is determined by iteration.

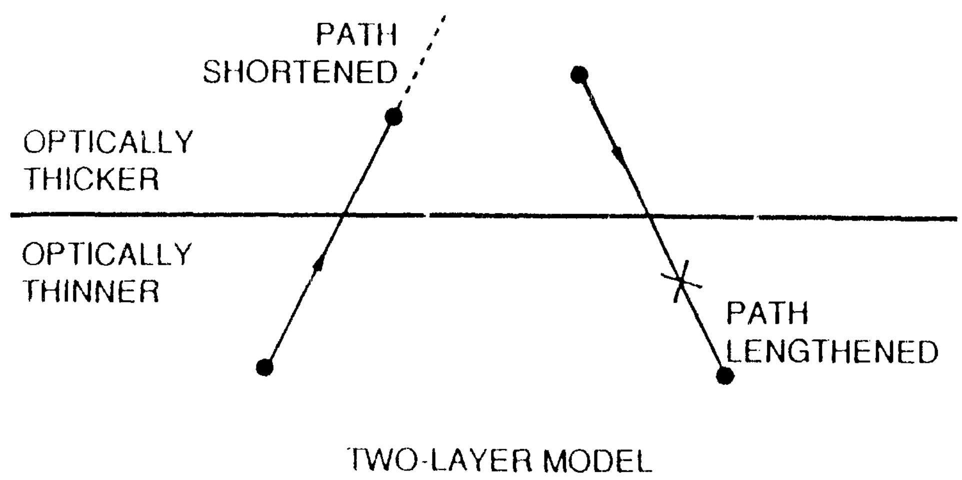

Figure A-6. Mean Free Path

$$d\Omega = \sin\theta \, d\theta \, d\phi = d\,(\cos\theta)\, d\phi$$

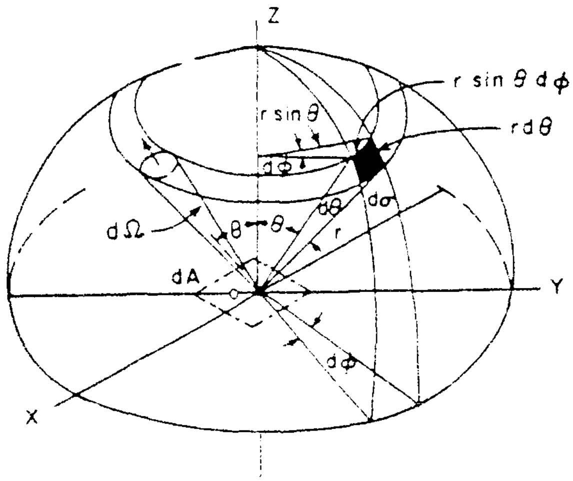

Figure A-7. Scattering Geometry

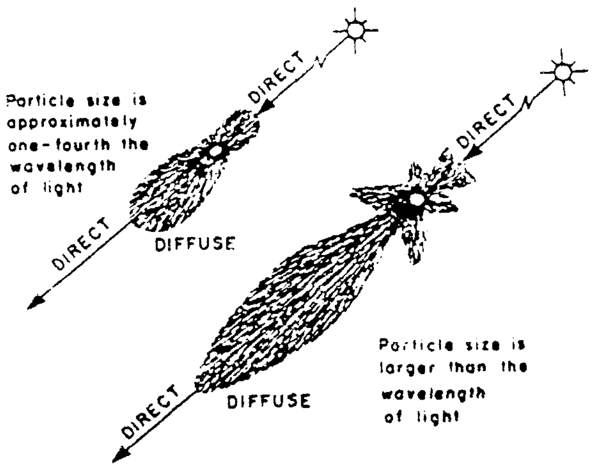

Note:
Complex scattering pattern is caused by the interaction of electromagnetic waves with molecular dipoles characterized by strong forward scattering.

Figure A-8. Schematic of Mie Scattering

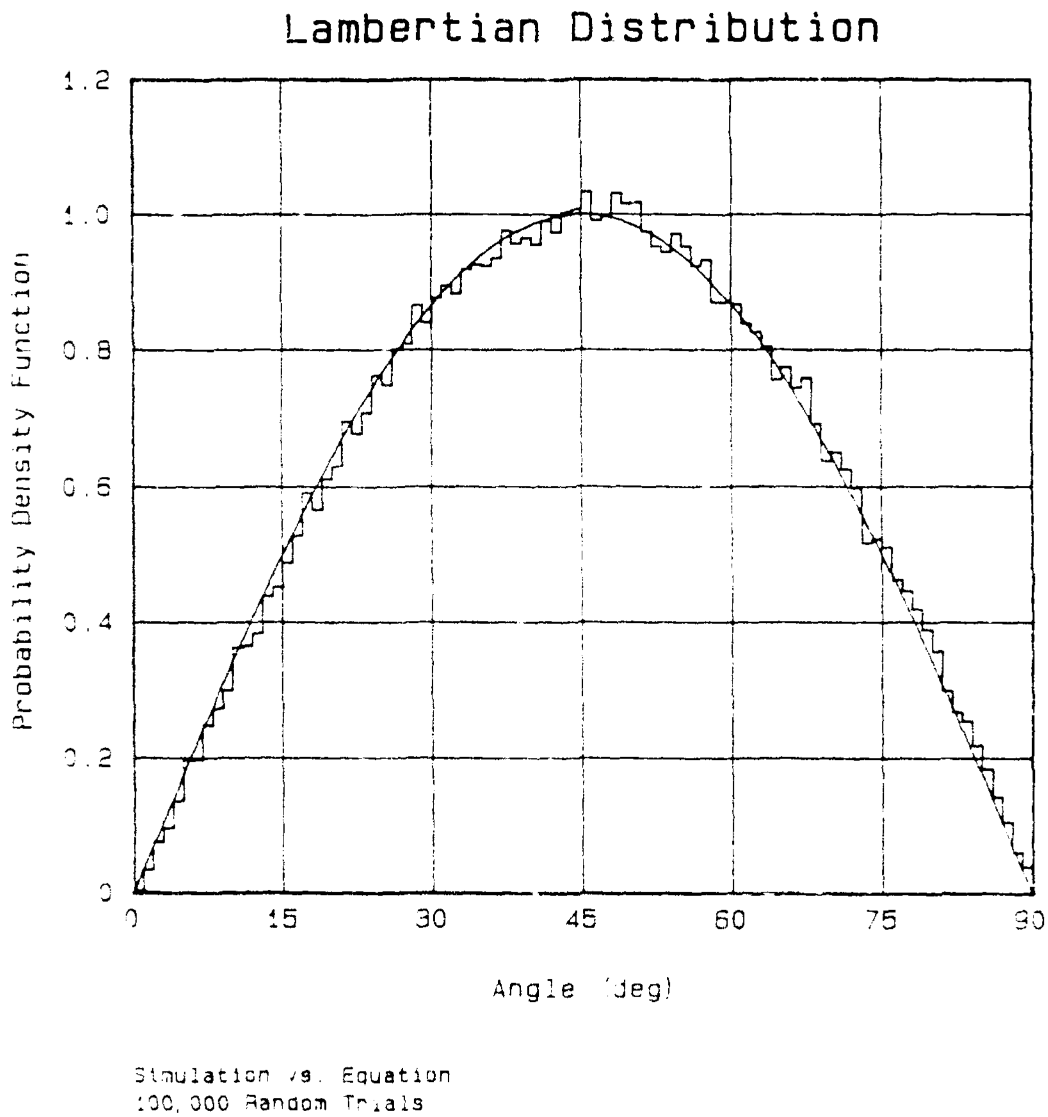

Figure A-9 Comparison of Simulation and Equation:
Lambertian Distribution

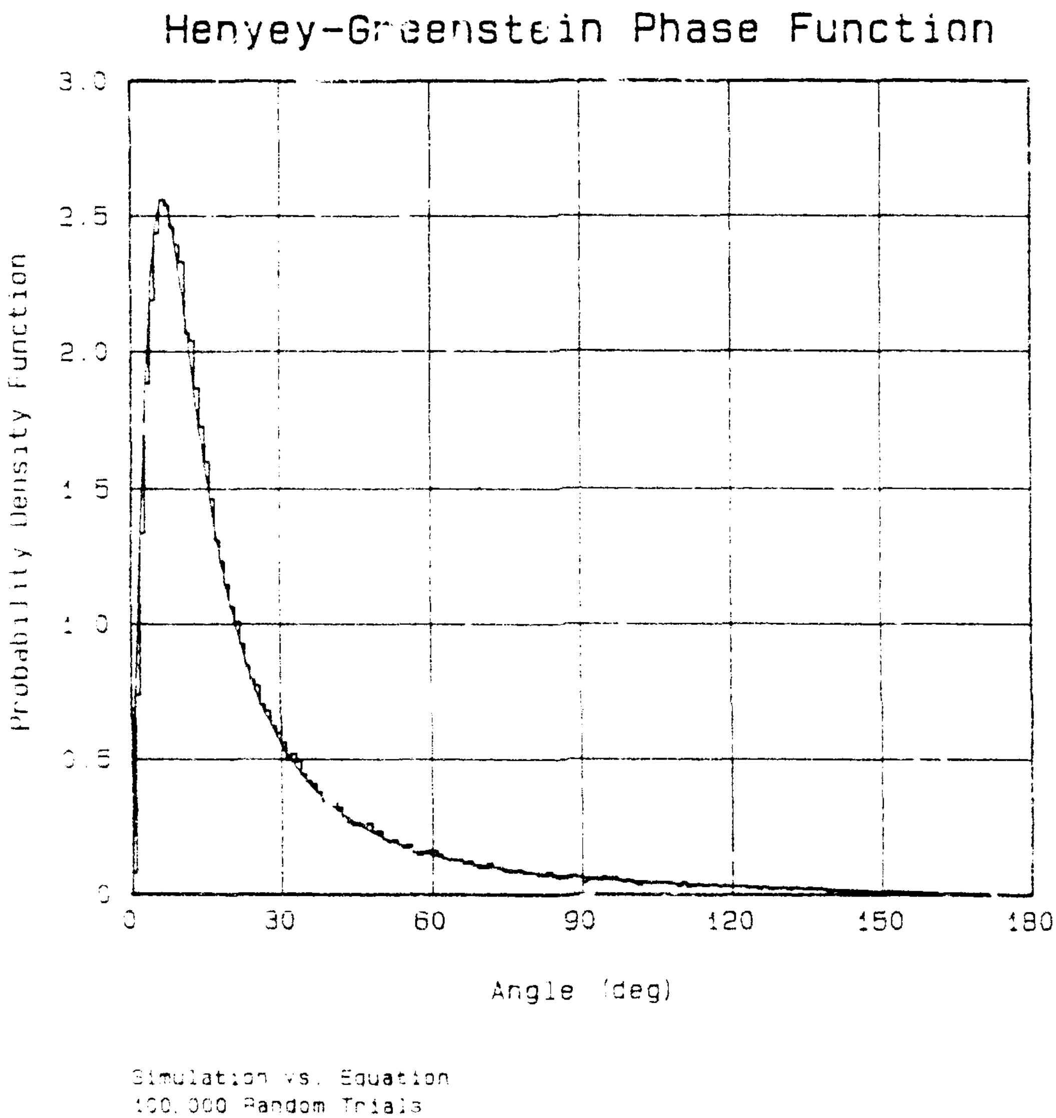

Figure A-10. Comparison of Simulation and Equation.
Henyey-Greenstein Distribution

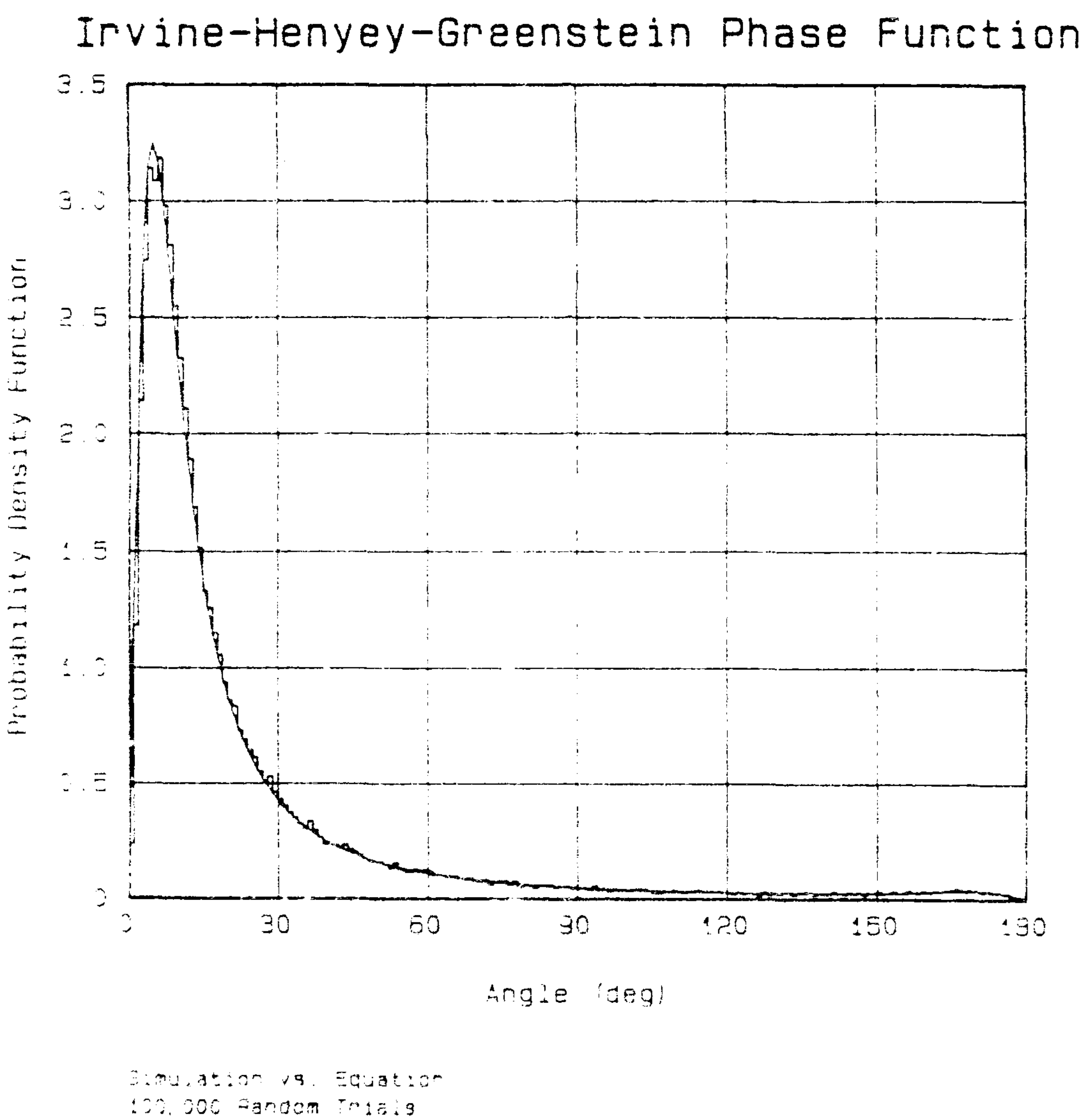

Figure A-11. Comparison of Simulation and Equation:
Irvine-Henyey-Greenstein Distribution

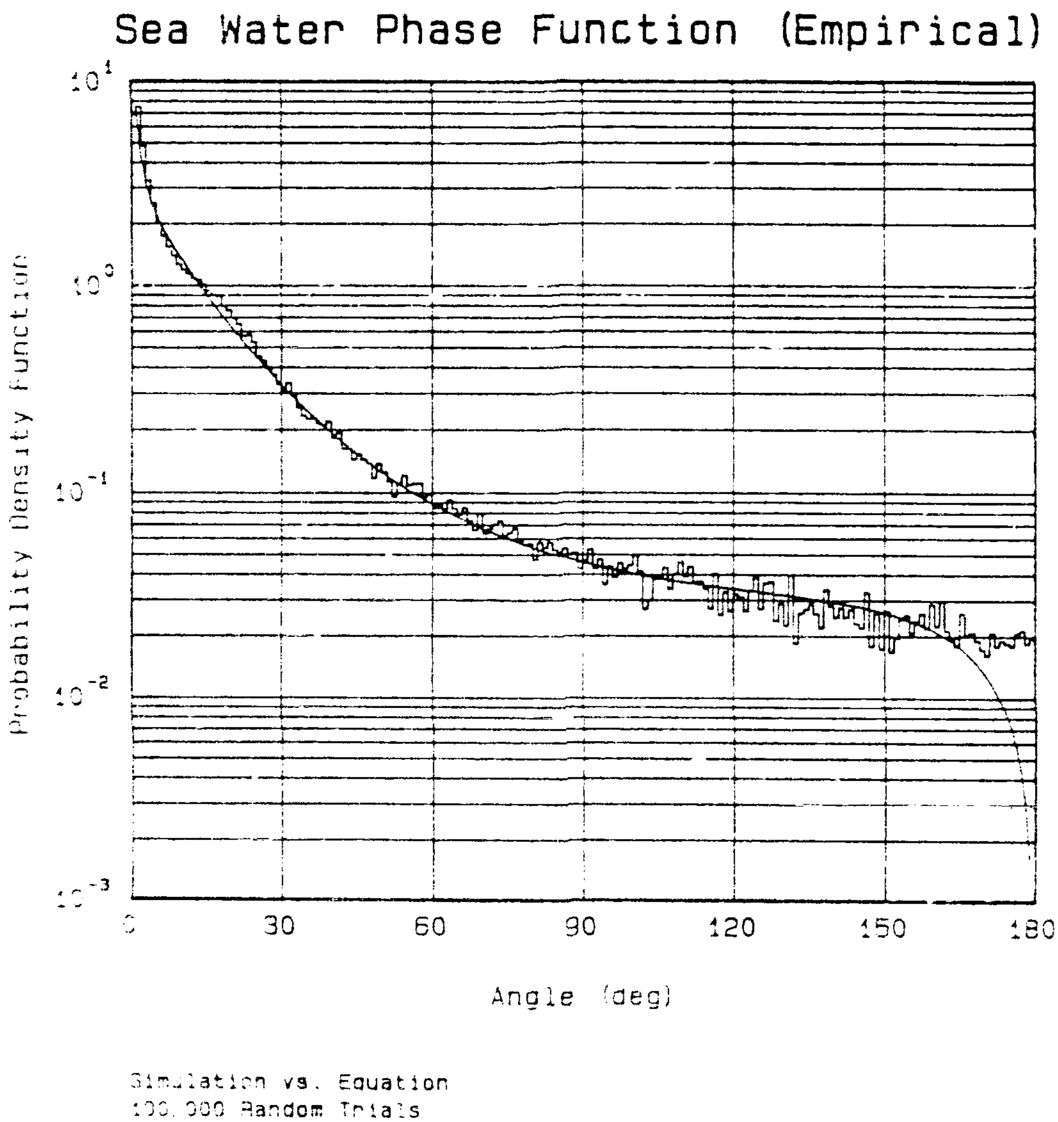

Figure A-12. Comparison of Simulation and Equation:
Sea Water Distribution

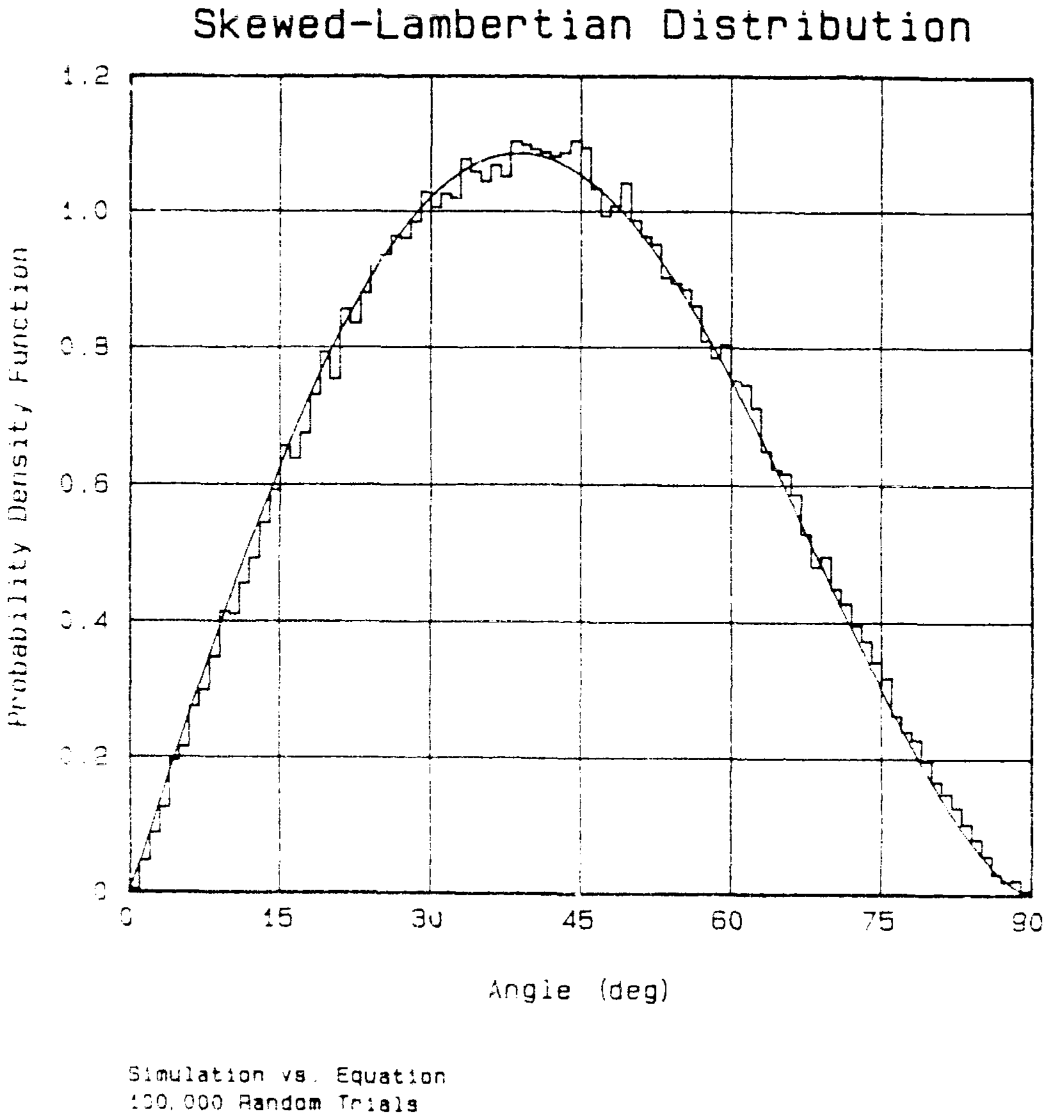

Figure A-13. Comparison of Simulation and Equation:
Skewed Lambertian Distribution

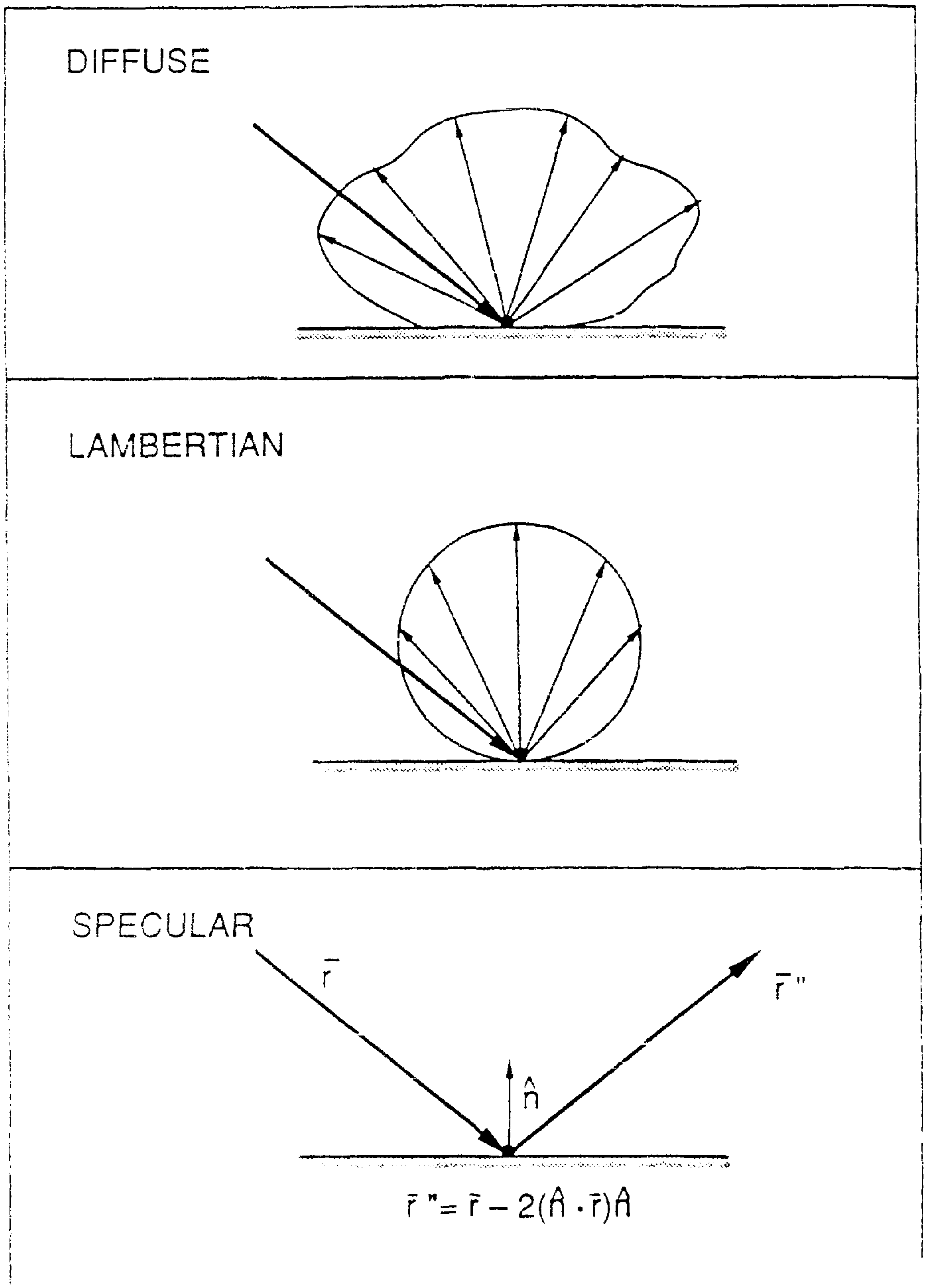

Figure A-14. Surface Reflection

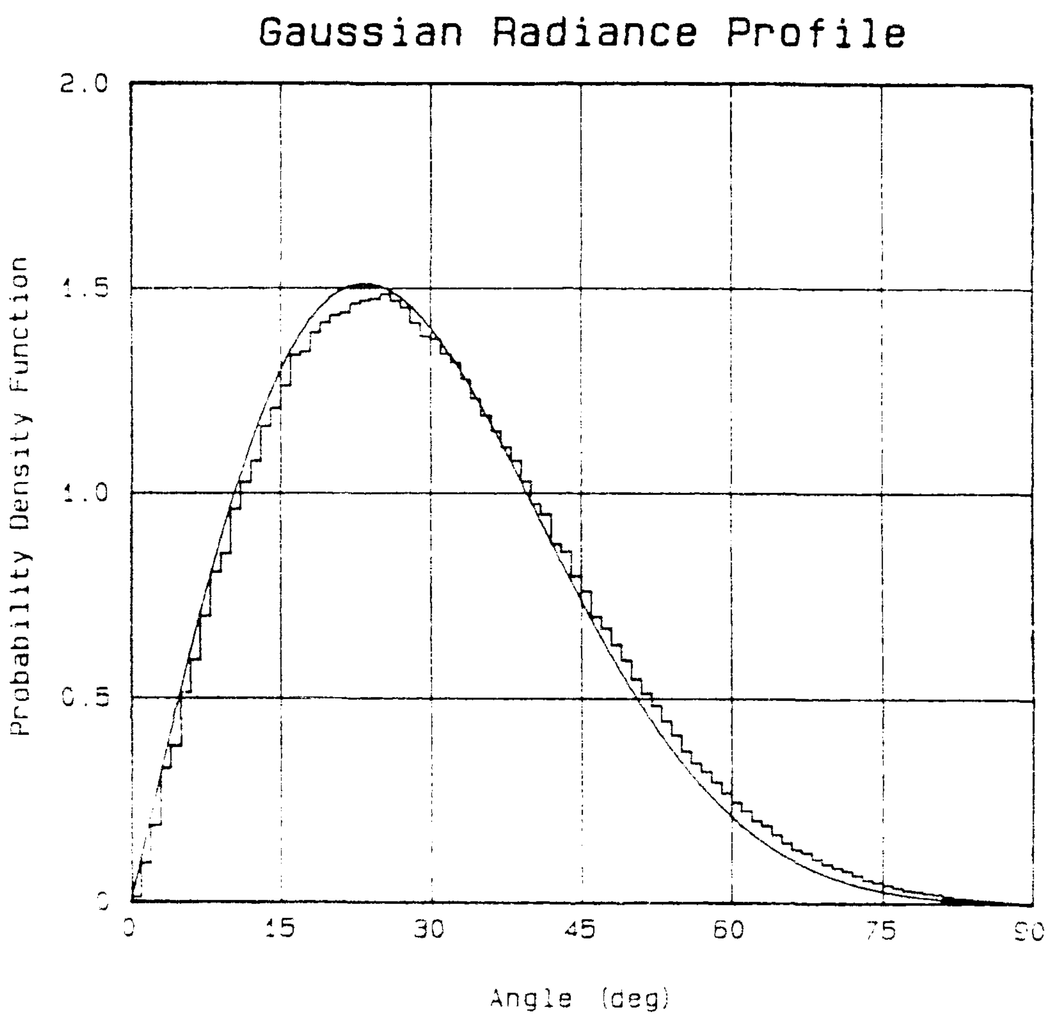

Simulation vs. Equation
(simulation uses approx
gauss radiance profile)

Receiver fov = 90 deg

1.0E+6 Random Trials

Figure A-15. Comparison of Simulation and Equation:
Gaussian Radiance Distribution

APPENDIX B. INTENSITY REFERENCE METHOD FOR RADIATIVE TRANSFER

1.0 INTRODUCTION

The purpose of this Appendix is to give a brief description of the intensity reference method. The method has been described by Meier, Lee, and Anderson (1978) and will be reviewed briefly here along with a description of a model extension for cases where the photon is near the receiver. Basically, there are three distinct domains of interest which are referred to as far-field, mid-field, and near-field depending upon the distance of the photon to the detector. The technical discussion contains a brief description of each of these.

In the intensity reference method the probability of reaching the detector is computed and stored at each photon scattering. The accumulated probabilities are then proportional to the intensity, as described below. Photons continue to follow their natural histories as determined by the specified physical processes. The advantage of this scheme is that, in contrast to the low likelihood of a photon actually hitting a receiver, there will always be some probability of it actually occurring. Thus, summing the probabilities greatly improves the statistics since each scattering event contributes to the intensity. In addition, the probability is computed exactly from the scattering point to the receiver; no other approximations are introduced. Moreover, the technique lends itself to vignetted receivers, i.e., receivers with a limited field of view (which lowers the likelihood of a photon hitting the detector even further).

2.0 TECHNICAL DISCUSSION

The intensity reference method considers the probability of the photon reaching a detector as a consequence of a scattering event. Figure B-1 shows a schematic drawing of the method. The probability of a photon being scattered in the direction of the detector is

$$p(\theta) = \int_{\omega} P(\theta_s) d\omega \qquad \text{(B-1)}$$

where the integration is bounded by the solid angle from the scattering event to the receiver area. However, along the path to the detector the photon may be absorbed or scattered out of the path. Thus, the probability of the photon actually reaching the receiver is diminished. In addition, the photon "weight" upon scattering is accounted for so that the probability is finally given by

$$p = \int_{\omega} w P(\theta_s) e^{-(\alpha+\beta)d} \, d\omega \tag{B-2}$$

where w is the initial photon weight, α and β are the absorption and scattering coefficients, respectively, and d is range from the scatterer to the differential solid angle. Equation (B-2) is a two-dimensional integration and is numerically cumbersome .

2.1 Far-field Approximation

The far-field approximation is frequently employed in radiative transfer problems. It is applicable when the detector area is small compared with the square of the range; in other words, for small solid angles. In that case, Eq. (B-2) becomes

$$p = w P(\theta_s) e^{-(\alpha+\beta) z / \cos\zeta} \, \Delta\omega \tag{B-3}$$

where

$$\Delta\omega = \frac{A_r \cos\zeta}{d^2} = \frac{A_r \cos^3\zeta}{z^2} \tag{B-4}$$

and θ_s is the scattering angle given by

$$\cos\theta_s = \bar{l}_1 \cdot \bar{l}_2 \tag{B-5}$$

where $\bar{l}_1$ is the direction cosine (unit vector) of the scattering point, $\bar{x}_i$ and $\bar{l}_2$ is the direction cosine of the photon arriving at $\bar{x}_i$. This is the most common application of the intensity reference method. It's particularly useful in atmospheric problems where the distances are large and the receivers are small.

2.2 Mid-field Calculation

The far-field approximation breaks down when the photon is sufficiently close to the receiver because the solid angle can no longer be approximated by Eq. (B-4). Thus, recourse must be made to Eq. (B-1). For a circular receiver Eq. (B-1) can be written as

$$p = \int_0^{2\pi} \int_0^{R} \frac{w P(\theta_s) e^{-(\alpha+\beta)d}}{d^2} \cos\zeta \; r \, dr \, d\theta \tag{B-6}$$

where R is the receiver radius. The distance, d, the scattering angle, θ_s, and the zenith angle, ζ, are all functions of the independent variables r and θ. Comparisons of computations with Eqs. (B-3) and (B-6) show that Eq. (B-3) is suitable if the range is about ten times the receiver radius. Generally speaking, Eq. (B-6) is not suitable for inclusion in Monte Carlo simulations but should not be ruled out altogether.

2.3 Near-field Approximation

As the photons get closer to the receiver the accuracy required of the integration increases, thus slowing it down. This occurs at a height above the receiver of about one-tenth of the radius. In that close range the solid angle is very nearly 2π (one-half of the total solid angle). Thus, the integral can be approximated as follows:

$$p = w\left(\frac{b+f}{2} + \frac{b-f}{2} l_3\right) \tag{B-7}$$

where absorption and scattering have been neglected (the intensity reference method wouldn't make sense if the medium was so optically dense at that distance to the receiver), l_3 is the direction cosine of the arriving photon, and f and b are the forward and backward scattering *functions, viz.*,

$$f = 2\pi \int_0^1 P(\mu)\,d\mu \tag{B-8}$$

$$b = 2\pi \int_{-1}^0 P(\mu)\,d\mu \tag{B-9}$$

Equation (B-7) is clearly correct when the photon is headed straight up ($l_3 = 1$, $p = wb$), straight down ($l_3 = -1$, $p = wf$), and straight across ($l_3 = 0$, $p = w/2$) so it's probably reasonable for any value of direction cosine.

3. CONCLUSIONS

The intensity reference method is a powerful tool for Monte Carlo simulations and should be used where it is applicable.

4.0 REFERENCE

Meier, R.R., Lee, J-S., and Anderson, D.E. (1978). "Atmospheric Scattering of Middle UV Radiation from an Internal Source," Appl. Optics, 17, No. 20, pp 3216-3225.

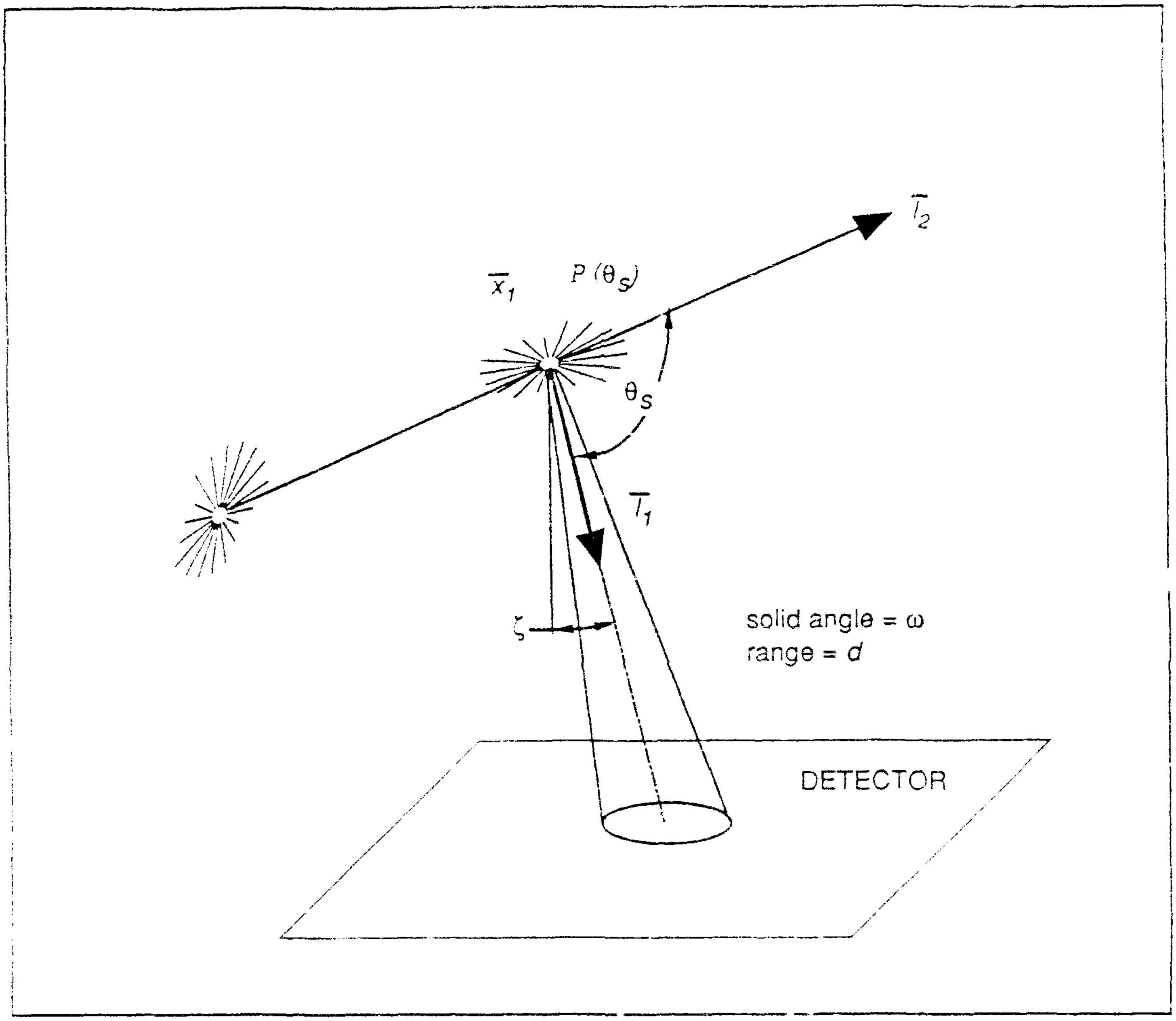

Figure B-1. Schematic of Intensity Reference Method

APPENDIX C. MODIFIED GAMMA FUNCTION PULSE

The modified function is frequently used as a model for the temporal pulse spreading of scattered radiation. The purpose of this Appendix is to collect the appropriate relations for the pulse time to peak, mean, rms, and 3dB pulsewidth. The pulse is expressed as a probability density function

$$p(t) = k^2 t\, e^{-kt} \tag{C-1}$$

where k is the inverse characteristic time. The distribution function is then

$$f(t) = \int_0^t p(t)\,dt = 1 - (1 + kt)e^{-kt} \tag{C-2}$$

so that $f(0) = 0$ and $f(\infty) = 1$. The time to peak is given by

$$\frac{dp(t)}{dt} = 0; \qquad t_{peak} = \frac{1}{k} \tag{C-3}$$

The mean time is given by

$$\bar{t} = \int_0^t t\,p(t)\,dt = \frac{2}{k} \tag{C-4}$$

The rms time is given by

$$t_{rms} = \int_0^t (t - \bar{t})^2\, p(t)\,dt = \frac{\sqrt{2}}{k} \tag{C-5}$$

or

$$t_{rms} = \int_0^t (\bar{t})^2\, p(t)\,dt = \frac{\sqrt{6}}{k} \tag{C-6}$$

The 3dB pulsewidth is given by the difference in times where $p(t) = p(0)/2$; this must be solved by iteration, there results

$$t_{3dB} = \frac{2.446386039257 05}{k} = \frac{\sqrt{6}}{k} \tag{C-7}$$

The views and conclusions contained in this report are those of the contractors and should not be interpreted as representing the official policies, either expressed or implied, of the Naval Ocean Systems Center or the U.S. Government.

Approved for public release, distribution is unlimited.